Title

INTERACTION BETWEEN LAMINAR BOUNDARY LAYERS AND SHOCK WAVES WITH SEPARATION OF FLOW

A Thesis

SUBMITTED TO THE GRADUATE FACULTY

OF THE UNIVERSITY OF MINNESOTA

by

W. W. Koepcke, Lieutenant U. S. Navy

In Partial Fulfillment of the Requirements

for the Degree of

Master of Science in Aeronautical Engineering

May 1957

ACKNOWLEDGMENTS

The author wishes to express his appreciation to Dr. Rudolf Hermann, Professor of Aeronautical Engineering, University of Minnesota, for his interest, encouragement, and advice in the development of the project; to Mr. Frederick Moynihan, principal engineer, Rosemount Aeronautical Laboratories, for his timely suggestions during the wind tunnel operating period; to Mr. Miles Mock, machinist in the Department of Aeronautical Engineering, who fabricated the working models; and to his wife for her understanding and patience throughout the entire period of the author's postgraduate study.

W. W. K.

TABLE OF CONTENTS

INTERACTION BETWEEN LAMINAR BOUNDARY LAYERS AND SHOCK WAVES WITH SEPARATION OF FLOW

1. SUMMARY

Shock waves generated by a 5° and a 10° half angle wedge located in the main stream of a Mach ~ 3.0 test section were impinged on the laminar boundary layer of a flat plate causing separation of flow. The flow was considered to be two dimensional with zero heat transfer. Reynold's numbers, from 150,100 to 1,098,000, were produced by varying length along the flat plate, and by changing stagnation pressure. Analysis was mainly accomplished through the study of static pressure profiles, supplemented by shadow photographs.

Important results were:

(1) The ratio of the pressure at the separation point, and the pressure just upstream of the sharp pressure rise denoting separation was nearly constant regardless of magnitude of shock, and did not vary with Reynold's number.

(2) The ratio of the pressure at the top of the laminar foot (region of nearly constant pressure within the interaction zone upstream of shock impingement point) and the pressure just upstream of the interaction region varied inversely with Reynold's number to the (.12) power.

(3) The ratio of the interaction distance upstream to the boundary layer thickness varied inversely with Reynold's number to the ($\frac{1}{2}$) power.

As many as five inflection points were found in the pressure profile of a laminar boundary layer acted upon by a shock wave. In general, step type shock waves showed consistency while impulse type shock waves showed inconsistency with a variation of parameters. Evidence was presented showing different results according to whether Reynold's number variation was obtained by changing length or stagnation pressure.

The experimental study was carried out at the Rosemount Aeronautical Laboratories, University of Minnesota during the school year 1956-1957 in conjunction with Lt. E. E. Irish, U. S. Navy, who investigated turbulent boundary layers utilizing approximately the same configuration.

INTERACTION BETWEEN LAMINAR BOUNDARY LAYERS AND SHOCK WAVES WITH SEPARATION OF FLOW

2. INTRODUCTION

This investigation was conducted principally to bring out features of the interaction between shock waves, strong enough to cause separation, and laminar boundary layers on a flat plate. The analysis was concentrated chiefly on the static pressure distribution on the flat plate supplemented by shadow photographs.

The equipment was designed so that the effects of a pressure gradient caused by a shock wave would be observed on a body in supersonic flow. The shock wave was generated by means of wedges, of varying half angles, suspended in the main stream of a supersonic tunnel. The wave impinged on a flat plate below the wedge. In this manner since the flat plate had initially a zero pressure gradient along its upper surface, the effects of the externally imposed shock

wave on the flat plate's boundary layer could be observed. The boundary layer was always laminar upstream of the zone of interaction. Surface roughness of the flat plate was minimized, Mach number was held nearly constant, and zero heat transfer was assumed. The wedge was moved streamwise within the test section resulting in the shock wave impinging at different locations on the flat plate. Thus, the parameters varied were Reynold's number, by varying both length and total pressure; and shock strength. The flat plate and wedge completely spanned the test section thereby simulating two-dimensional flow.

This experimental investigation was carried out at the Rosemount Aeronautical Laboratories, Department of Aeronautical Engineering, University of Minnesota during the school year 1956-1957 in conjunction with Lt. E. E. Irish, U. S. Navy, who conducted experiments of the same general nature with turbulent boundary layers.

3. TABLE OF SYMBOLS

d - corrected interaction distance upstream of the theoretical shock wave impingement point on the flat plate (d' corrected for static hole diameter).

d' - measured interaction distance upstream of theoretical shock wave impingement point on the flat plate

h - diameter of static pressure taps in flat plate

I - theoretical shock wave impingement point on the flat plate

M_I - Mach number of flow at shock wave's impingement point on the flat plate

M_o - Mach number at the upstream beginning of interaction

P - total or stagnation pressure

p - static pressure within the interaction zone

p_o - static pressure just upstream of the interaction zone

p_s - static pressure at the separation point

p_T - static pressure on top of the laminar foot, denoted by second inflection point (T) in the pressure profile curve

psia - pounds per square inch absolute

psig - pounds per square inch gage

R_I - Reynold's number at the shock wave's impingement point on the flat plate

R_o - Reynold's number based on the distance from the leading edge of the flat plate to the point where the pressure begins to rise (beginning of upstream interaction)

S - first inflection point in the pressure profile curve denoting separation point

T - second inflection point in the pressure profile curve

X_I - distance from leading edge of flat plate to shock wave's impingement point on the flat plate

X_o - distance from leading edge of the flat plate to the upstream beginning of interaction

δ_I - boundary layer thickness at the point where the shock wave impinged on the flat plate calculated assuming no added thickening due to the shock wave

δ_o - boundary layer thickness at the upstream beginning of interaction

δ_o^* - displacement thickness of the boundary layer at the upstream beginning of interaction

4. EQUIPMENT

To study the interaction between the boundary layer on a flat plate, and shock waves produced externally outside the boundary layer, half angle wedges were suspended in the main stream of a supersonic wind tunnel. Shock waves of varying strengths generated by these wedges were projected onto the boundary layer of a flat plate mounted within the test section.

The continuous flow supersonic wind tunnel utilized was located at the Rosemount Aeronautical Laboratories, facilities of the Department of Aeronautical Engineering, University of Minnesota. Air was delivered to the stilling chamber of the tunnel from a 1750 cubic foot pressure storage tank (240 psig capacity). The air was dried to -40° F dew point before delivery from the compressor to the storage tank. The compressor was three staged with a capacity of 195 cubic feet per minute at 1500 psig. Downstream of the tunnel was a vacuum system consisting of a 30 foot diameter sphere (14,000 cubic feet) plus five cylindrical tanks (total volume 8,750 cubic feet). The system could be evacuated to a pressure of $\frac{1}{2}$ in. mercury, absolute. The test section was 1.75 in. wide

by 1.94 in. high with an asymmetric nozzle block designed for Mach 3.05, (Fig. 1a). The upper portion of the block was made of lucite and furnished the curvature providing the expansion to the design Mach number. This half was designed to compensate for boundary layer growth. The lower part of the block was straight, did not compensate for boundary layer growth and was made of steel. The working section had circular glass side walls approximately 3 in. in diameter, thereby permitting photography of the flow.

The flat plate, 4½ in. long, completely spanned the tunnel and was anchored to the lower tunnel wall by means of a 0.715 in. high, 0.125 in. thick steel pylon. The plate was made of stainless steel; was hardened and had a commercial plating of chrome 0.0001 in. thick to reduce surface roughness. It had a 5° half wedge angle at the leading edge and was 0.125 in. thick at the maximum point. The leading edge thickness was 0.0010 in. There were five static pressure holes staggered along the center line of the flat plate. The most forward hole was 0.725 in. from the leading edge. Each succeeding hole was 0.250 in. further downstream, the fifth hole being 1.725 in. from the leading edge. Each hole was 0.006 in. in diameter. Leading from each hole beneath the plate was a

copper tube 1/16 in. in diameter. The tubes ran along the lower side of the plate downstream into the diffuser section of the tunnel and then out to a manometer board. The tubing was continuous from a solder attachment at the bottom of each hole until joining the plastic tubing of the board. (See Figs. 1b and 1c for a schematic drawing and photograph of the flat plate).

The wedges which generated the shocks impinging on the flat plate's boundary layer completely spanned the tunnel and were suspended from the upper nozzle block by means of a steel pylon 0.2 in. in height, and 0.125 in. thick.

The pylon in turn fitted in a "T" slot cut into the upper block, the slot being 0.125 in. wide running along the longitudinal center line of the upper block. The pylon was attached to a lead screw which extended downstream through a flange connecting the test section and diffuser. The lead screw (40 threads per inch) was turned by means of a small ratchet wrench. The wedge thus could be moved streamwise within the test section, and was always parallel to the upper nozzle block surface. Fig. 1d is a photograph showing the test section, the ratchet wrench and lead screw mechanism, and the pylon which supported the wedge.

Two wedges were used in the laminar flow runs for generating the shocks. One had a 5° half angle and the other a 10° half angle. Both were 1/8 in. thick at the maximum point. The 5° wedge's leading edge was .0006 in. thick, the 10° leading edge was .0011 in. thick. See Fig. 2a for a photograph of the two wedges. See Fig. 2b for a drawing of the 10° wedge imposing a shock wave onto the flat plate.

Total temperature within the stagnation chamber was measured by means of thermocouple leads connected to a potentiometer (manufactured by Leeds and Northrup Co.). The thermocouple within the chamber was shielded by a plastic covering.

Six static pressures, five from the holes on the flat plate, (location shown on Fig. 1b) and one from a hole in the lower tunnel wall upstream of the flat plate were measured within the test section. The static pressure hole in the lower tunnel wall, about one inch upstream of the leading edge of the flat plate was only utilized in determining starting of the tunnel, and as an aid in checking for choking within the test section. These six holes or orifices were connected to a multiple tube mercury manometer, which also had tubes exposed to atmospheric pressure for reference readings. The barometric pressure was taken before each series of runs by means of a standard brass mercury barometer. Parallel light

shadow photographs were taken by means of a BH-6 power source and a mercury arc lamp with a columinated light beam and with a flash of approximately three microseconds.

5. PROCEDURE

For the laminar flow runs, two stagnation pressures of about 14.7 psia and 45 psia were used to obtain a variation in Reynold's number from 150,100 to 1,098,000. With the lower pressure, Reynold's number varied along the five holes on the flat plate from 150,100 to 355,000. With the higher pressure, the variation was from 456,000 to 1,098,000. Reynold's number was held constant by varying total pressure with each change in total temperature of 10° Fahrenheit.

For each series of runs (either low pressure or high pressure) a static pressure reading of the six orifices was taken with the shock generating wedge in its most downstream position. The wedge was then advanced upstream in regulated intervals by means of a calibrated lead screw. The tunnel was not operated in a continuous flow manner. The sequence was to advance the wedge, start the tunnel, shut off the mercury manometer tubes by means of a clamping device when pressures were steady, shut down the tunnel, read the total temperature and the mercury column heights, advance the wedge, and begin the sequence again. The wedge was advanced forward generally until the most forward hole on the flat plate had reached a pressure peak. At this time, the series was completed.

6. PRESENTATION OF RESULTS

Tables I to IV show important results obtained from the pressure profiles of each tap hole. These tables include interaction distances; pressure ratios of separation, and at the top of the laminar foot; Reynold's numbers. Tables V to IX show the static pressure measurements in inches of mercury absolute for each hole on the flat plate for the 5° wedge, 45 psia runs with reference to the wedge's position from its most downstream position in the test section. Figs. 3 to 12 show the static pressure profiles for Reynold's numbers varying from 150,100 to 1,098,000 as generated by the 5° wedge. Figs. 13 to 22 show the same profiles and Reynold's number variation as generated by the 10° wedge. Fig. 23 is a log-log plot of $\frac{d}{\delta_o^*}$ versus (R_o) for the 5° and 10° wedge. Fig. 24 is a log-log plot of $\frac{d}{\delta_I}$ versus (R_I) for the 5° and 10° wedges. Fig. 25 is a log-log plot of $\frac{P_T}{P_o}$ versus (R_o) for the 5° and 10° wedges. Fig. 26, 27, 28, and 29 are a series of shadow photographs showing the shock waves generated by the 5° and 10° wedges impinging on the flat plate at various Reynold's numbers. Fig. 30 shows Mach number distribution within the test section at each hole with the wedges in the most downstream (zero reference) position.

The pressure profiles were plotted with $\frac{p}{p_o}$ as the ordinate where p_o was the static pressure of each hole when the wedge was in its most downstream position (wedge position = zero inches in Tables V to IX) In this manner, the profiles then show how the initial pressure at each hole was disturbed as the wedge was advanced upstream. Each of the pressure profiles presented in this report (Figs. 3-22) thus show the pressure at a single static hole as the shock wave advanced from a position downstream and passed over the hole, i.e., Fig. 3 shows the pressure profile obtained as the 5° wedge, impinging a shock wave onto the flat plate's boundary layer, was advanced from a position approximately one inch downstream of the most upstream hole on the flat plate until the shock wave passed over and upstream of the hole. The abscissa of the pressure profiles is always the wedge's position with reference to its most downstream (zero) station in inches.

This method had certain distinct advantages:

(1) To get as many data points as are shown on the pressure profiles by impinging the shock at only one point would have required a large number of static pressure holes.

(2) Some of the small pressure differences measured probably would have been completely lost because of the difference in pressure that could be expected within the test section between holes.

However some error could be introduced by reflection of tunnel waves from the wedge as it moved forward. Also the closer one approached the leading edge of the flat plate, the more error one might introduce because of the lack of constant characteristics of a boundary layer in that region.

The series of shadow photographs (Figs. 26-29) show the state of the boundary layer as the shock wave was directly over each hole. It should be noted that the pressure profiles do not necessarily represent the exact conditions of the boundary layers as shown by the shadow photographs, but if boundary layer characteristics did not vary too widely over the flat plate, then the profiles show a close approximation of the actual conditions.

Tables V to IX have been included to show the data for the 5° wedge, 45 psia runs for each hole. From these tables, Fig. 8 to 12 were constructed. The remaining pressure profiles were constructed in the same manner from similar data.

7. DISCUSSION

7.1 Theoretical and Historical Background

Boundary layer-shock wave interaction affected one of the most significant concepts in fluid flow, Prandtl's theory of the boundary layer. Prandtl's basic assumption was that viscous stresses in a low viscosity fluid were small compared to other terms in the momentum equation except in a relatively thin layer near solid boundaries. Here large velocity gradients occurred and thus significant viscous stresses existed. These viscous effects were ignored in calculations involving the flow external to the layers near the boundaries. This was an outstanding simplification provided the boundary layer flow did not appreciably affect the external flow. For then the two regions of flow were calculated separately; the external flow as though it were non-viscous and without heat conduction with its boundary assumed to be the solid object in the stream, and then the viscous effects at the wall according to boundary layer theory. If the boundary layers were thin compared to a dimension of the solid body, then it was shown that the boundary layer had only a second order effect on the exterior flow, this effect principally being an outward displacement of potential flow streamlines due to the displacement thickness of the boundary layer.

The principal assumptions of boundary layer theory are that the rates of change of velocity and temperature perpendicular to a bounding surface are large compared to rates of change in a direction parallel to the flow. In a shock wave on the other hand the reverse is true. Pressure, temperature, and velocity gradients perpendicular to the wave are large compared with changes parallel to the wave. When a shock wave occurs near a solid body, so that there is an interaction between the boundary layer and shock wave, the two are in basic conflict.

Thus the simple boundary layer theory is broken down, for the interaction between the boundary layer and shock wave produces first order effects affecting both the external and the boundary layer flow. The shock wave imposes such a large pressure gradient upon the boundary layer that it is distorted. It has been found that this distortion in turn causes additional compression and expansion waves to be generated from the boundary layer into the external flow which changes the original shock pattern. The interaction between a shock wave and a boundary layer leads to a flow pattern different from one which is predicted by simple shock wave theory and boundary layer theory separately.

Attention was first drawn to the effects of boundary layer, shock wave interaction by Ferri (Ref. 1) who during tests in a supersonic tunnel observed boundary layer separation near the trailing edge of a wing section at a point where a favorable pressure gradient was expected. He stated, "On the side of the wing on which there is expansion and which should therefore have a compression shock at the trailing edge, there is observed in every case a phenomenon not predicted by theories, namely that before reaching the trailing edge, there is a sudden pressure increase, well brought out in the photographs, by a shock wave which separates two regions of very different luminosity." Although in most practical cases today, turbulent flow prevails, the chances of extensive laminar boundary layers seem to be growing as planes and rockets fly to greater altitudes. With decreasing density the Reynold's number decreases which enhances the possibility of extensive laminar boundary layers (Ref. 2).

7.2 Preliminary Discussion of the Experimental Results

Two types of shock waves were generated in the experiment, the 5° wedge creating a "step-type" shock, and the 10° an "impulse-type" shock wave. There were marked differences in the two types. See section "Impulse and Step Shock Waves"; also Fig. 31, for definition of the two types of shock waves. The pressure profiles and results shown in the tables for the 5° wedge generally agreed with those in Ref. 3, that interaction distances upstream for initially laminar boundary layers generated by a wedge of about a 5° half angle are approximately 50 boundary layer thicknesses. The Ref. 3 runs were conducted at Mach 1.5; the present report at Mach 3.0. Interaction distances for the 10° wedge reached 70 boundary layer thicknesses upstream. Peak static pressures, in agreement with Ref. 3, were slightly higher than theoretical for the 5° wedge and were considerably lower than theoretical for the 10° wedge. Pressure profiles, with as many as five inflection points were found in certain instances, confirming results of Ref. 4. The quantity $\frac{d}{\delta_o^*}$ was found to vary as $R_o^{-\frac{3}{4}}$ for Reynold's numbers within the known laminar flow range for the 5° wedge, while the 10° results of the same quantities were inconsistent.

The quantity $\frac{d}{\delta_I}$ was found to vary as $R_I^{-\frac{1}{2}}$ for the 5° wedge over the known laminar flow range. The quantity $\frac{d}{\delta_I}$ for the 10° wedge varied inconsistently with R_I. Every pressure profile within the laminar flow range showed separation. The pressure ratio $\frac{p_s}{p_o}$ did not appear to vary with Reynold's number nor with the strength or type of shock, impulse or step. The pressure ratio $\frac{p_T}{p_o}$ varied approximately with $R_o^{-.14}$ for both types of shocks. Shadow photographs showed the point of actual shock impingement on the flat plate to agree approximately with the theoretical impingement point for the 5° and 10° wedge. The primary shock was, however, bent visibly as it approached the flat plate, thus creating doubt as to the reliability of the pressure profile to accurately pin point the impingement. No doubt exists however, in laminar flow as to the tremendous smearing of the high pressure behind the shock wave upstream through the boundary layer.

7.3 Upstream Interaction Distance

Tables I through IV show the interaction distance (d) upstream of the shock's impingement point on the flat plate with respect to the displacement thickness δ_o^* at the point where interaction began upstream. (This ratio was used extensively in Ref. 4).

The point was always taken to be at the initial pressure rise in the pressure profile. The quantity (d') was the actual distance measured upstream at which pressure began rising and (h) was the diameter of the static pressure hole. The diameter of the hole (h) was subtracted from the measured interaction distance (d') to get the true interaction distance (d). In this manner, the effect of the diameter of the hole in increasing the upstream distance was cancelled. This method was taken from Ref. 15, which showed good experimental results because of this correction. The displacement thickness was calculated from the formula in Ref. 5:

$$\delta_o^* = 1.72\ (1 + 0.277\ M_o^2)\ \frac{X_o}{R_o^{\frac{1}{2}}} \quad \text{where}$$

δ_o^* = displacement thickness of the boundary layer at the upstream beginning of interaction

X_o = distance from leading edge of the flat plate to the beginning of interaction

M_o = Mach number at the upstream beginning of interaction

The boundary layer thickness was calculated from the formula in Ref. 6:

$$\delta_I = \left[5.2 + 1.03\ (\gamma - 1)\ M_I^2\right] \frac{X_I}{R_I^{\frac{1}{2}}} \quad \text{where}$$

δ_I = boundary layer thickness at the point where the shock wave strikes the flat plate

X_I = distance from leading edge of flat plate to shock impingement point on plate

M_I = Mach number at the shock impingement point

For $M_o = M_I = 3$

$$\delta_o^* = 6.0 \frac{X_o}{R_o^{\frac{1}{2}}}$$

$$\delta_I = 8.9 \frac{X_I}{R_I^{\frac{1}{2}}}$$

In Ref. 3, Liepmann discussed the interaction distance (d) in terms of the boundary layer thickness and Reynold's number where the shock wave theoretically impinged on the flat plate. This interaction definition is shown in Table I through IV in the column $\frac{d}{\delta_I}$. See Appendix B for sample calculations with this method. The method of Ref. 4 simplifies calculations considerably in contrast to Ref. 3, since one needs to determine the Reynold's number for each tap hole once, and it remains the same. In the method of Ref. 3 however, one must calculate the Reynold's number at each point the shock wave strikes the boundary layer or flat plate. Both methods will show trends with Reynold's number but the method of Ref. 3 seems to be preferable for practical application since it gives variation with the Reynold's number of the boundary layer where the shock strikes, and not at a point where the shock is felt upstream.

For a 5° wedge, the values of $\frac{d}{\delta_I}$ were comparable to those found in Ref. 3 for a $4\frac{1}{2}$° wedge, and (d) was found to be approximately 50 boundary layer thicknesses. It is to be noted that the experimental runs of Ref. 3 were conducted at Mach = 1.5, while in the present report, the runs were at Mach = 3.0. For the 10° wedge, the distances were increased up to 70 boundary layer thicknesses depending on Reynold's number. Log-log plots of $\frac{d}{\delta_o^*}$ and $\frac{d}{\delta_I}$ versus Reynold's number are shown in Fig. 23 and 24 and are discussed in the section "Transition in the Interaction Zone".

The theoretical position of the shock wave striking the flat plate was shown on each pressure profile figure with the symbol (I). The pressure peak always occurred downstream of the position (I). In general, more of the total pressure rise occurred upstream of the position (I), in the case of the impulse type shock than the step type shock wave. This seemed reasonable for the total pressure rise of the impulse shock type had been blunted by the expansion wave; consequently the position (I) would appear to move downstream relative to the pressure profile. This result also corresponded with Ref. 3 differentiating impulse and step shock waves. One should

note that it is practically impossible to pinpoint the actual impingement of the shock wave by observing the pressure profile. In the laminar case, the smearing of the shock wave's pressure causes rapid thickening and sometimes transition upstream. If the transition was not too pronounced, it would not be observable on the profile (see discussion on "Inflection Points on a Pressure Profile") as an inflection point, but would still influence the gradient enough to apparently cause the steep pressure gradient near the shock wave to move further upstream. At other times, transition could occur far enough upstream of the primary shock to cause an added inflection point in the profile, (see Fig. 22). One thus could only pinpoint the actual shock impingement as being located somewhere on the profile where the steepest gradient occurred.

7.4
Inflection Points on a Pressure Profile

In Ref. 4 the author stated that under certain conditions, an initially laminar flow, acted upon by a shock wave would show five inflection points within the pressure profile. Beginning from the point where a rise in pressure was first noted the points in successive order would denote:

(1) Separation

(2) Transition

(3) Thickening of the turbulent layer

(4) Shock impingement

(5) Reattachment of flow downstream of shock

The five inflection points would occur if transition were a considerable distance ahead of the shock. Fig. 22 shows five inflection points where the pressure profile of hole number five, 1.725 in. from the leading edge at a stagnation pressure of about 45 psia and a Reynold's number of 1.098 (10^6) has been plotted to two longitudinal scales. Also on Fig. 22 is a pressure profile of hole number one, 0.725 in. from the leading edge of the flat plate at a total pressure of about 101 psia and a Reynold's number of 1.01 (10^6). The profiles are very similar showing a definite break in the curve at $\frac{p}{p_o} \sim 1.9$. This inflection point is masked on a shortened longitudinal scale. The pressure profiles in Ref. 3 in general did not show this break, probably due to the extremely shortened scale. Since the profiles of holes one and five at about the same Reynold's number show the five inflection points, Ref. 4 appears to be substantiated. The author (Ref. 4) explains the five points in the following manner:

1. There is first a foot where the boundary layer is laminar and the pressure falls off after separation because the separated region becomes thick.

2. When transition occurs, the boundary layer although separated can withstand a larger pressure gradient and the pressure rises steeply.

3. The dead air region (separated region) becomes very thick further downstream so that the pressure gradient must fall again since even the turbulent friction forces cannot withstand a large gradient.

4. When the shock strikes the boundary layer the flow is deflected towards the wall, the separated region becomes thinner, and the pressure gradient rises.

5. Reattachment of the boundary layer occurs near the peak pressure position and the gradient falls off once more as the pressure profile approaches its final downstream form.

In most instances within the present report however, only three inflection points were observed, presumably because the boundary layer did not thicken enough between transition and shock for the pressure gradient to be visibly affected or else transition did not occur until shock impingement on the boundary layer.

7.5 Impulse and Step Shock Waves

An impulse shock wave is defined to be of the type where the generated shock wave is produced by a flow deflection angle closely followed by a generated expansion wave, produced by the same magnitude flow deflection angle. A step shock wave is defined to be of the type where the expansion wave does not occur within the interaction distance downstream of the impingement point of the shock wave on the flat plate. See Fig. 31, a sketch showing the difference in the two types of shocks. Within this report, the 5° wedge created an expansion wave which theoretically impinged on the flat plate 0.91 in. downstream of the shock wave. Since interaction distances upstream of the shock wave were approximately one inch, 5° wedges were assumed to generate step waves. The 10° wedges however generated expansion waves which theoretically impinged on the flat plate 0.15 in. downstream of the shock wave, thus generating impulse type shock waves. As shown on Figs. 3 to 12, the 5° wedge created pressure peaks which were always greater than theoretical, and the 10° wedge created pressure peaks always lower than theoretical (Figs. 13 to 22) throughout the range of Reynold's numbers tested. Of particular

note is Fig. 17(b) which is Fig. 17 (a) plotted to a different horizontal scale and extended beyond the pressure peak. It shows that the pressure returned to a position below initial pressure i.e., that there was an over expansion. The results above were in agreement with those of Ref. 3 and corroborated the general characteristics of an impulse type wave. Step shock wave pressure data did not show this over expansion. Theoretical pressure peaks were defined to be those stream pressures attained downstream of the shock pattern of a given oblique shock wave if it struck the flat plate and was regularly reflected in the absence of a boundary layer. In the case of the 5^{o} wedge with an initial Mach 3 flow:

$$\frac{p_{final}}{p_{initial}} = 2.04$$

In the case of the 10^{o} wedge, with Mach 3 flow:

$$\frac{p_{final}}{p_{initial}} = 3.93$$

The above values were calculated by charts in Ref. 7.

7.6 Transition Within the Interaction Zone

An effort was made to create an entirely laminar flow throughout the region of interaction, upstream and downstream, even with flow separation. In Ref. 4, this was only achieved (at Mach 2) with a wedge of 6^{o} and Reynold's numbers below 150,000. Results of Ref. 4 showed that for completely laminar flows the quantity $\frac{d}{\delta_o^*}$ graphed versus R_o showed a positive slope. When transition occurred within the zone of interaction, $\frac{d}{\delta_o^*}$ varied as $R_o^{-\frac{1}{3}}$ over a range of R_o from 2 (10^5) to 4 (10^5), i.e., the graphical slope was negative.

In the present investigation $\frac{d}{\delta_o^*}$ versus R_o was graphed on a log-log plot over a range varying from 150,100 to 1,098,000 for the 5^{o} wedge. To achieve the Reynold's numbers from 150,100 to 355,000, tunnel stagnation pressure over the five holes on the flat plate was approximately 14.7 psia. For the higher range, stagnation pressure was about 45 psia. The two series of runs are shown on Fig. 23. The lower Reynold's number series showed a variation of $\frac{d}{\delta_o^*}$ with $R_o^{-\frac{3}{4}}$. The higher series showed a variation of $\frac{d}{\delta_o^*}$ with $R_o^{-\frac{3}{4}}$, with the slope showing a tendency to become less steep for the Reynold's numbers above 776,000.

Note on Fig. 23 that there is a discontinuous jump in the curves rather than a straight line continuation when the stagnation pressure was changed. An explanation of the possible cause of this discontinuous jump follows:

In Ref. 12, a complete resume' of the transition to turbulent boundary layers at supersonic speeds, the author stated that transition extends over a finite distance and depends on:

(a) Conditions of the test stream

(b) Conditions of the leading edge of the test body

(c) Thermal conduction in the test body

Taking case (a) first, (Conditions of the test stream), several experimenters have noted a systematic increase of transition Reynold's number with an increase of stagnation pressure (Ref. 12) i.e., as Reynold's number per length increased, so did the Reynold's number of transition. The increase was proportional to the stagnation pressure increase, since stagnation temperature was approximately the same. If one speculates on the possible consequences of the change of stagnation pressure and Reynold's number per unit length, the following effects present themselves:

(1) A decrease of R_x per unit length increases the length of the laminar part of the boundary layer. This increases the total extent of the effect of disturbances in the test section and surface roughness, and hence tends to reduce the Reynold's number of transition.

(2) The thickness of the boundary layer is larger in the case of the lower R_x per unit length for any given length, δ = (constant) $\frac{x}{R_x^{\frac{1}{2}}}$. Therefore the boundary layer is more susceptible to outside disturbances. Thus the lower R_x per unit length, the more chance that a disturbance causes earlier transition.

In the present experiment then, when the stagnation pressure was changed from 14.7 to 45 psia, for the same Reynold's number, a hole nearer the leading edge of the flat plate would show characteristics more typical of a laminar boundary layer than a hole further downstream. The hole most upstream would thus show a greater $\frac{d}{\delta_o^*}$ ratio, assuming that laminar flows always show greater interaction $\frac{d}{\delta_o^*}$ ratios than turbulent flows. This is precisely what occurred in the experiment. On Fig. 23, the discontinuous jump occurred when Reynold's number was changed from 356,000 to 456,000

by increasing total pressure and shifting from hole 5, the furthest downstream, to hole 1, closest to the leading edge.

Taking case (b), conditions at the leading edge of the test body, it has been noted that there is a systematic decrease of transition Reynold's number with reduction in thickness of the leading edge of a test body due to vibrations, (Ref. 12). Assuming that vibration of the leading edge occurred, the higher the stagnation pressure, the more vibrations per second, and thus the possibility of earlier transition.

In the present experiment however, when stagnation pressure was increased, for approximately the same Reynold's number, the boundary layer acted more like a laminar one than one undergoing transition. Therefore, vibrations were not the cause of the discontinuous jump in Fig. 23.

Taking case (c), thermal conditions in the test body, it has been noted in many tests that a rise of recovery temperature occurred near the leading edge due to thermal conduction within the test body. (Ref. 12). In the present experiment in order to get desired strength, the nose of the flat plate was built in the form of a wedge with the top surface parallel to the stream. The wedge thus causes a lower Mach number on its surface and consequently a higher temperature on the lower surface. Conduc-

tion in the nose wedge would then cause a higher observed recovery temperature on the upper surface. Since the temperature was higher on the nose of the upper surface, this could lead to a greater degree of instability of the boundary layer than if the nose were cooler.

However in the present experiment, stagnation temperature was very nearly the same regardless of the stagnation pressure. Therefore, the effects of possible thermal conduction within the test body should have been the same regardless of pressure.

In evaluation of the three possible causes, it would appear that case (a), conditions of the test stream, was the most likely reason for the discontinuous jump in Fig. 23.

With regard to the tendency for the change of slope at R_o of 776,000, previous investigators (Ref. 13) utilizing the same wind tunnel as the present report found that natural transition began taking place at about R_o of 800,000. Likewise Fig. 12, a pressure profile at a Reynold's number of 1,098,000, did not show a separation point, whereas the other profiles within the same series were consistent in this aspect. The separated region may have been too small to appear on the profile. However it would be reasonable to assume, that once the

flow entered the natural Reynold's number realm of transition, that inconsistent results from either wholly laminar or wholly turbulent flow would result, and in this instance the flow did not separate. Ref. 12 also stated that parameters affecting flows which were in a natural transition status were still very far from being understood. Hence, the present report although showing the pressure profiles for R_o of 936,000 and 1,098,000, in general disregards the data since there is justified doubt as to their being stable laminar flows.

In order to decide whether or not completely laminar flow had been attained, the shadow photographs were scrutinized, the pressure profiles were examined and references were checked. The photographs were not discernable enough in this respect. If the pressure profiles showed five inflection points, this would have indicated transition. In the range of Reynold's numbers from 150,100 to 355,000, all of the profiles showed only three inflection points. In Ref. 4, and reiterated again by the same author in Ref. 14, Fig. 7, completely laminar flow was only accomplished below a Reynold's number of 150,000 at Mach 2 with a 6° wedge. The slope of $\frac{d}{\delta_o}$* versus R_o was positive in that case.

In the present investigation, the lowest Reynold's number was 150,100, and $\frac{d}{\delta_o^*}$ varied with $R_o^{-\frac{3}{4}}$ i.e., slope was negative. It was therefore concluded that pure laminar flow had not been achieved, and that transition probably occurred at the point of shock impingement or just downstream.

The quantity $\frac{d}{\delta_o^*}$ versus R_o was plotted on Fig. 23 for the 10° wedge also. For the lower Reynold's numbers, the variation was in good agreement with the 5° wedge results. In the upper R_o range, the slope was considerably steeper. In Ref. 5, the author stated that defective results were obtained when the compression wave was too closely followed by an expansion. This corresponds to the present case for the 10° wedge, which generated an impulse shock wave.

The quantity $\frac{d}{\delta_I}$, discussed in the "Interaction Distance" section was plotted versus R_I on Fig. 24. An arbitrary slope of $(-\frac{1}{2})$ was superimposed through the data points. The 5° wedge results showed the same break in the curve upon a shift of stagnation pressure as noted earlier, and with a tendency to vary away from the slope, above R_I of 776,000 although not as pronounced as noted before. The 10° wedge results were not as consistent; there was more scatter, and a change in slope with a change of stagnation pressure. This again was in agreement with

other results, that an impulse type shock produces inconsistent results for many quantities compared to a step type shock.

7.7
Separation

Evidence of separation occurred in every pressure profile for an initially laminar flow except Fig. 12. This discrepancy is more fully discussed in the section, "Transition Within the Interaction Zone". It is sufficient to note here that Fig. 12 is a pressure profile of a flow at a Reynold's number of 1,098,000. At this Reynold's number, the flow probably was in a state of natural transition and may not have been a valid laminar profile.

In Ref. 8, Fig. 2, separation was defined to be the point where the first inflection point occurred in the pressure curve. In Ref. 9 the separation region was defined to be the position on the profile curve where the pressure was nearly constant. Both definitions are in agreement, the former more precise as to the onset of separation. In Ref. 4, evidence was presented to show that separation of laminar flow did not occur if the half angle wedge generating the shock was smaller than 2^{o}. In the non-separated cases, the pressure profile only showed one inflection point at about the position of the shock impingement. In

the present report, the wedges utilized had half angles of 5° and 10°, the pressure profiles within the laminar range had at least three inflection points - the flows were separated.

Theories have been advanced as to the ratio value between p_s, pressure at the separation point, and p_o, stream pressure just upstream of the sharp pressure rise denoting separation. In Ref. 10, for laminar flow, the author predicted, at Mach 3 and R_o of $2.5(10^5)$, that $\frac{p_s}{p_o}$ would equal 1.18. Ref. 8 stated that the ratio value depended on the external flow Mach number and state of the boundary layer, either laminar or turbulent. For undisturbed flows definitely within the laminar range of Reynold's numbers, the pressure ratio causing separation at Mach 3 would be approximately 1.14.

In Ref. 5, the point of separation was measured experimentally with a half Pitot tube with values of $\frac{p_s}{p_o} = 1.14$ at Mach 3, although the value was qualified with the statement that the exact separation point was very difficult to detect. The ratio did not vary over the range of Reynold's numbers tested, $2\ (10^5)$ to $4\ (10^5)$.

In the present report, testing with both the 5° and 10° wedges in a Reynold's number range from 150,100 to 776,000, results were in good agreement with the above ratio of Ref. 5. Taking the first point of inflection on the pressure profiles as p_s,

the following resulted:

$$1.08 \leq \frac{p_s}{p_o} \leq 1.17$$ with a mean value of 1.12. There was no consistent variation with Reynold's number. However, selecting the exact point of inflection on the curves was somewhat nebulous, and a consistent variation with Reynold's number may not have been perceived. In Ref. 10, theory predicted a variation of $\frac{p_s}{p_o}$ with $R_o^{-\frac{1}{4}}$, and in Ref. 11, the prediction was a variation with $R_o^{-\frac{1}{2}}$. Ref. 10 advanced the following theory toward $\frac{p_s}{p_o}$: "When a sufficiently strong oblique shock wave is incident upon the boundary layer on a flat plate, it causes both the pressure to increase and the boundary layer to thicken and separate upstream of it. The thickening of the boundary layer generates a band of compression waves that determine the pressure distribution acting on the boundary layer upstream of the shock, and this pressure distribution in turn governs the rate of thickening of the boundary layer. The two processes must adjust themselves to be in equilibrium so that the pressure distribution upstream of a certain point where a shock impinges on a boundary layer would presumably remain unaltered if the shock were increased in strength and simultaneously moved downstream to some new point such that the separation point did not move. Hence the ratio of pressure

at separation to the undisturbed free stream pressure should be a function of Mach number and Reynold's number only, independent of shock strength."

The present report appears to substantiate in part the above theory, for $\frac{p_s}{p_o}$ did not appear to vary regardless of strength nor type of shock, impulse or step, while interaction distance upstream changed depending on shock strength and Reynold's number. However, a consistent variation of $\frac{p_s}{p_o}$ with Reynold's number was not observed.

7.8
Pressure at the Top of the Laminar Foot

In Ref. 8, the author defined the second inflection point on the pressure profile as the top of the laminar foot. The laminar foot is defined as the region of relatively small pressure gradient between the shock wave's impingement point and the most upstream interaction point. This laminar foot is the outstanding feature distinguishing laminar from turbulent pressure profiles. In Ref. 5, a graph of $\frac{p_T}{p_o}$, pressure at the top of the laminar foot (second point of inflection) over pressure of the undisturbed stream was shown versus Reynold's number. In log-log coordinates, $\frac{p_T}{p_o}$ varied with $R_o^{-.11}$ for a range of R_o from 100,000 to 400,000. On Fig. 24, $\frac{p_T}{p_o}$ versus R_o for the present report is shown with the results of Ref. 5. The variation with R_o agrees well with Ref. 5,

except for R_o above 776,000 for the 10° wedge. Again, for flows which in the absence of the shock are known to be laminar, correlation of results is good.

For the 5° wedge, $\frac{p_T}{p_o}$ varied approximately with $R_o^{-.11}$ as in Ref. 5. For the 10° wedge, $\frac{p_T}{p_o}$ varied with $R_o^{-.16}$ from 150,100 to 776,000. Apparently the variation with R_o was consistent regardless of type of shock wave, impulse or step. In this case also, when stagnation pressure was changed, there was a discontinuous jump in the curves, as in the discussion section on "Transition Within the Interaction Zone".

7.9
Shadow Photographs

Figs. 26 to 29 are shadow photographs of the conditions existing within the test section during the experimental runs. The pictures were not intended to be utilized for their quantitative value, but were initially used to check flow configuration because of choking difficulties. They did show the characteristic thickening of the boundary layer due to the interaction, and certain aspects pointed out below.

For the 5° wedge runs, Figs. 26 and 27, the photographs show that the actual shock impinged close to the theoretical position on the flat plate. The pictures were taken at the wedge position when the theoretical impingement point was over each hole. In

looking at the photographs one can observe the tubing leading from each hole under the flat plate. Each hole is almost directly vertical to the upstream edge of the tubing. The tubing was braced with a solder backing and thus looks much thicker than its 1/16 in. actual diameter.

The 10° wedge runs, Figs. 28 and 29, show that the primary shock was deviated (bent) much more than the 5° wedge shocks. This could have been due to:

(1) More intense compression shocks from the relatively thicker boundary layer upstream.

(2) Expansion fan effect off the rear of the wedge, which caused the 10° shock to be originally defined as an impulse type.

One would believe however that the compression shocks emanating from the region of separated boundary layer were the main factor because the primary shock wave showed a sharp kink when it deviated, rather than a gradual bend, typical of expansion wave reaction.

The photographs showed evidence of a shock wave at the leading edge of the flat plate. This leading edge compression shock in the case of the 5° wedge configuration (Fig. 25(e)) was mild, as shown by static pressure measurements. The Mach number immediately forward of the flat plate was 2.99, while

on the flat plate, the average Mach number was about 2.95 (Fig. 30). Assuming the leading edge shock wave caused the drop in Mach number, the intensity would have been that caused by a flow deviation of less than one degree. However since pressure profiles were graphed always as the ratio of the static pressure for each hole, when the wedge was in its most rearward position, to that pressure as the wedge was advanced, the leading edge disturbance was essentially cancelled out.

The bending of the shock wave would have affected the apparent interaction distance upstream, because this distance was always measured relative to the theoretical impingement point of a clean shock wave generated off the leading edge of the wedge. The ratio $\frac{p_s}{p_o}$ would not be affected by the bending because it is primarily dependent on equilibrium between the undisturbed flow and thickening of the boundary layer, and not on the position of the shock wave.

8. CONCLUSIONS

A step shock wave generated by a 5° wedge and an impulse shock wave generated by a 10° wedge located in the main stream of a Mach $\sim$ 3.0 test section were impinged on the laminar boundary layer of a flat plate causing separation of flow. The flow was two-dimensional; Reynold's number varied from 150,100 to 1,098,000; zero heat transfer was assumed. Important results were:

(1) $\frac{d}{\delta_I}$ varied with $R_I^{-\frac{1}{2}}$ for the 5° wedge

(2) $\frac{d}{\delta_o^*}$ varied with $R_o^{-\frac{3}{4}}$ for the 5° wedge

(3) $\frac{p_s}{p_o} = (1.12 \pm .05)$ regardless of R_o

(4) $\frac{p_T}{p_o}$ varied approximately with $R_o^{-.14}$ for the 5° and 10° wedges

Although both types of pressure profiles showed laminar characteristics, the profile of the 5° wedge peaked at a value slightly higher than theoretical, while the profile of the 10° wedge peaked considerably lower than the theoretical value. In general, the step type shock wave was consistent, the impulse shock wave inconsistent, in parameter variations.

When Reynold's numbers were greater than 776,000, results were erratic, thus showing the beginning of natural transition. All flows, known to be laminar,

separated under the influence of the shock waves generated by the 5° and 10° wedges. There were no wholly laminar flows throughout the interaction region. Five inflection points were noted in certain pressure profiles denoting transition upstream of shock wave impingement on the boundary layer.

Evidence was presented in Figs. 23, 24, and 25 in the form of a discontinuous break in log-log curve plots showing that results were affected, depending on how a variation with Reynold's number was accomplished, by a change in length or a change in stagnation pressure.

REFERENCES

1. Ferri, A.: Experimental Results with Aerofoils in the High Speed Tunnel at Guidonia, NACA TM 946 (1940).
2. Young, D. D.: Boundary Layers and Skin Friction in High Speed Flow, Aeronautical Quarterly 1, page 137, (1949).
3. Liepman, H. W., A. Roshko, S. Dhawan: On the Reflection of Shock Waves from a Boundary Layer, NACA TN 2334 (1951).
4. Holder, D. W., H. H. Pearcey, G. E. Gadd: The Interaction between Shock Waves and Boundary Layers, Aeronautical Research Council No. 16,526 Current Paper No. 180 (1954).
5. Gadd, G. E., D. W. Holder, J. D. Regan: An Experimental Investigation of the Interaction Between Shock Waves and Boundary Layers, Royal Society of London Proceedings, 1954, Serial A 226 page 227.
6. Kuethe, A. M., J. D. Schetzer: Foundations of Aerodynamics, Wiley and Sons, 1950, page 301.
7. Dailey, C. L., J. C. Wood: Computation Curves for Compressible Fluid Problems, J. Wiley and Sons, 1949.

8. Gadd, G. E., D. W. Holder: Boundary Layer Separation in Two Dimensional Supersonic Flow, Aeronautical Research Council, Current Paper No. 270 (1956).

9. Shapiro, A. H.: The Dynamics and Thermodynamics of Compressible Fluid Flow, Volume II, pages 1141-1142, The Ronald Press Company, New York, (1953).

10. Gadd, G. E.: Interactions between Wholly Laminar or Wholly Turbulent Boundary Layers and Shock Waves Strong Enough to Cause Separation, Journal of the Aeronautical Sciences, November, 1953.

11. Donaldson, C., R. H. Lange: Study of the Pressure Rise Across Shock Waves Required to Separate Laminar and Turbulent Boundary Layers, NACA TN 2770 (1952).

12. Probstein, R. F., C. C. Lin: A study of Transition to Turbulence of Laminar Boundary Layers at Supersonic Speeds. Institute of the Aeronautical Sciences Preprint No. 596, January 1956.

13. Bradfield, W. S., D. G. DeCoursin, C. B. Blumer: Effect of Leading Edge Bluntness on Momentum Loss, Journal of the Aeronautical Sciences, June 1954.

14. Holder, D. W.: The Interaction Between Shock Waves and Boundary Layers. Institute of the Aeronautical

Sciences, Preprint No. 550, June 1955.

15. Moynihan, F.: Normal Shock - Boundary Layer Interaction Studies on Cones at Mach Number 1.5, University of Minnesota Rosemount Aeronautical Laboratories Research Report 136, October 1956.

TABLE I

TABULATED RESULTS

5° WEDGE, TOTAL PRESSURE 14.7 PSIA

Hole	1	2	3	4	5
X_o (inches)	0.725	0.975	1.225	1.475	1.725
R_o (10^{-5})	1.50	2.01	2.52	3.04	3.55
$\delta^*(10^3)$ (inches)	11.24	13.08	14.65	16.04	17.37
d' (inches)	1.053	1.053	1.025	0.953	0.853
d (inches)	1.047	1.047	1.019	0.947	0.847
$\frac{d}{\delta_o^*}$	93.0	80.1	69.6	59.0	48.8
$\frac{p_s}{p_o}$	1.12	1.17	1.11	1.11	1.12
$\frac{p_T}{p_o}$	1.24	1.22	1.18	1.18	1.18
$\frac{d}{\delta_I}$	40.1	37.5	34.7	30.9	27.0

TABLE II

TABULATED RESULTS

5° WEDGE, TOTAL PRESSURE 45 PSIA

Hole	1	2	3	4	5
X_o (inches)	0.725	0.975	1.225	1.475	1.725
R_o (10^{-5})	4.56	6.18	7.76	9.36	10.98
$\delta_o^*(10^3)$ (inches)	6.50	7.55	8.35	9.15	9.92
d' (inches)	0.653	0.603	0.553	0.553	0.553
d (inches)	0.647	0.597	0.547	0.547	0.547
$\frac{d}{\delta_o^*}$	99.5	79.0	65.5	59.8	55.0
$\frac{p_s}{p_o}$	1.11	1.13	1.14	1.10	--
$\frac{p_T}{p_o}$	1.22	1.20	1.17	1.13	--
$\frac{d}{\delta_I}$	49.4	42.5	36.6	34.2	32.5

TABLE III

TABULATED RESULTS

10° WEDGE, TOTAL PRESSURE $\sim$ 14.7 PSIA

Hole	1	2	3	4	5
X_o (inches)	0.725	0.975	1.225	1.475	1.725
R_o (10^{-5})	1.50	2.01	2.52	3.04	3.55
δ_o^* (10^3) (inches)	11.24	13.08	14.65	16.04	17.37
d' (inches)	1.377	1.277	1.227	1.152	0.902
d (inches)	1.371	1.271	1.221	1.146	0.896
$\frac{d}{\delta_o^*}$	122.	97.2	83.4	71.4	61.6
$\frac{p_s}{p_o}$	1.16	1.12	1.11	1.11	1.09
$\frac{p_T}{p_o}$	1.30	1.24	1.18	1.18	1.10
$\frac{d}{\delta_I}$	48.1	43.2	39.8	36.1	28.2

TABLE IV

TABULATED RESULTS

10° WEDGE, TOTAL PRESSURE $\sim$ 45 PSIA

Hole	1	2	3	4	5
X_o (inches)	0.725	0.975	1.225	1.475	1.725
R_o (10^{-5})	4.56	6.18	7.76	9.36	10.98
$\delta_o^*(10^3)$ (inches)	6.50	7.55	8.35	9.15	9.92
d' (inches)	1.027	0.877	0.677	0.677	0.577
d (inches)	1.021	0.871	0.671	0.671	0.571
$\frac{d}{\delta_o^*}$	157.	115.	80.3	73.3	57.6
$\frac{p_s}{p_o}$	1.14	1.10	1.10	1.08	1.13
$\frac{p_T}{p_o}$	1.22	1.14	1.12	1.14	1.18
$\frac{d}{\delta_I}$	68.6	57.3	43.9	40.9	33.7

TABLE V

$\frac{p}{p_o}$ VALUES FOR 5° WEDGE, P = 46.4 psia

HOLE 1

Wedge Position (inches)	p (inches mercury)	$\frac{p}{p_o}$
00000	2.57	1.00
1.625	2.57	1.00
1.675	2.57	1.00
1.725	2.60	1.01
1.775	2.65	1.03
1.825	2.72	1.06
1.875	2.85	1.11
1.925	2.96	1.15
1.975	3.03	1.18
2.025	3.08	1.20
2.075	3.11	1.21
2.125	3.13	1.22
2.175	3.13	1.22
2.225	3.13	1.22
2.275	3.19	1.24
2.325	3.24	1.26
2.375	3.44	1.34
2.425	4.22	1.64
2.475	5.40	2.10
2.525	6.09	2.37
2.575	6.20	2.41
2.625	6.15	2.39
2.675	6.04	2.35

p_o = 2.57 (inches mercury)

M_o = 3.00

TABLE VI

$\frac{p}{p_o}$ VALUES FOR 5° WEDGE, P = 46.4 psia

HOLE 2

Wedge Position (inches)	p (inches mercury)	$\frac{p}{p_o}$
00000	2.74	1.00
1.425	2.74	1.00
1.475	2.74	1.00
1.525	2.77	1.01
1.575	2.79	1.02
1.625	2.96	1.08
1.675	3.09	1.13
1.725	3.18	1.16
1.775	3.23	1.18
1.825	3.29	1.20
1.875	3.29	1.20
1.925	3.31	1.21
1.975	3.34	1.24
2.025	3.45	1.26
2.075	3.70	1.35
2.125	3.92	1.43
2.175	4.90	1.79
2.225	5.59	2.04
2.275	5.86	2.14
2.325	5.94	2.17
2.375	6.00	2.19
2.425	6.00	2.19
2.475	6.00	2.19
2.525	6.11	2.23
2.575	6.32	2.31
2.625	6.41	2.34

P_o = 2.74 (inches mercury)

M_o = 2.96

TABLE VII

$\frac{p}{p_o}$ VALUES FOR 5° WEDGE, P = 46.4 psia

HOLE 3

Wedge Position (inches)	p (inches mercury)	$\frac{p}{p_o}$
00000	2.66	1.00
1.275	2.66	1.00
1.325	2.66	1.00
1.375	2.69	1.01
1.425	2.77	1.04
1.475	2.85	1.07
1.525	3.03	1.14
1.575	3.11	1.17
1.625	3.27	1.23
1.675	3.62	1.36
1.725	4.07	1.53
1.775	4.57	1.72
1.825	5.18	1.95
1.875	5.74	2.01
1.925	6.04	2.27
1.975	6.09	2.29
2.025	6.04	2.27
2.075	5.98	2.25

p_o = 2.66 (inches mercury)

M_o = 2.98

TABLE VIII

$\frac{p}{p_o}$ VALUES FOR 5° WEDGE, P = 46.4 psia

HOLE 4

Wedge Position (inches)	p (inches mercury)	$\frac{p}{p_o}$
00000	2.83	1.00
0.975	2.83	1.00
1.025	2.83	1.00
1.075	2.83	1.00
1.125	2.89	1.02
1.175	2.97	1.05
1.225	3.11	1.10
1.275	3.17	1.12
1.325	3.20	1.13
1.375	3.28	1.16
1.425	3.48	1.23
1.475	3.79	1.34
1.525	4.53	1.60
1.575	5.04	1.78
1.625	5.41	1.91
1.675	5.63	1.99
1.725	5.83	2.06
1.775	5.89	2.08
1.825	5.89	2.08
1.875	5.83	2.06
1.925	5.77	2.04

p_o = 2.83 (inches mercury)

M_o = 2.94

TABLE IX

$\frac{p}{p_o}$ VALUES FOR 5° WEDGE, P = 46.4 psia

HOLE 5

Wedge Position (inches)	p (inches mercury)	$\frac{p}{p_o}$
00000	2.70	1.00
0.775	2.70	1.00
0.825	2.70	1.00
0.875	2.74	1.01
0.925	2.78	1.03
0.975	2.89	1.07
1.025	3.05	1.13
1.075	3.24	1.20
1.125	3.51	1.30
1.175	4.02	1.49
1.225	4.48	1.66
1.275	4.84	1.79
1.325	5.10	1.89
1.375	5.32	1.97
1.425	5.35	1.98
1.475	5.40	2.00
1.525	5.43	2.01
1.575	5.51	2.04
1.625	5.65	2.09
1.675	5.75	2.13
1.725	5.79	2.15
1.775	5.83	2.16
1.825	5.81	2.15
1.875	5.72	2.12
1.925	5.61	2.08

$p_o = 2.70$

$M_o = 2.97$

Fig. 1A

ASYMMETRIC NOZZLE BLOCK

FIG. 1B

FLAT PLATE

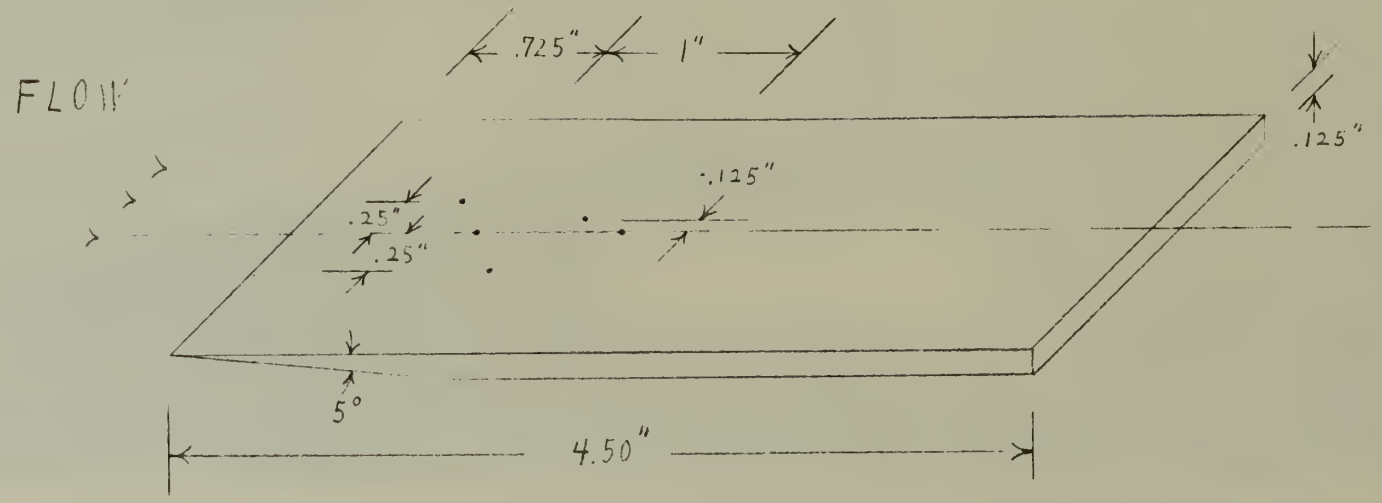

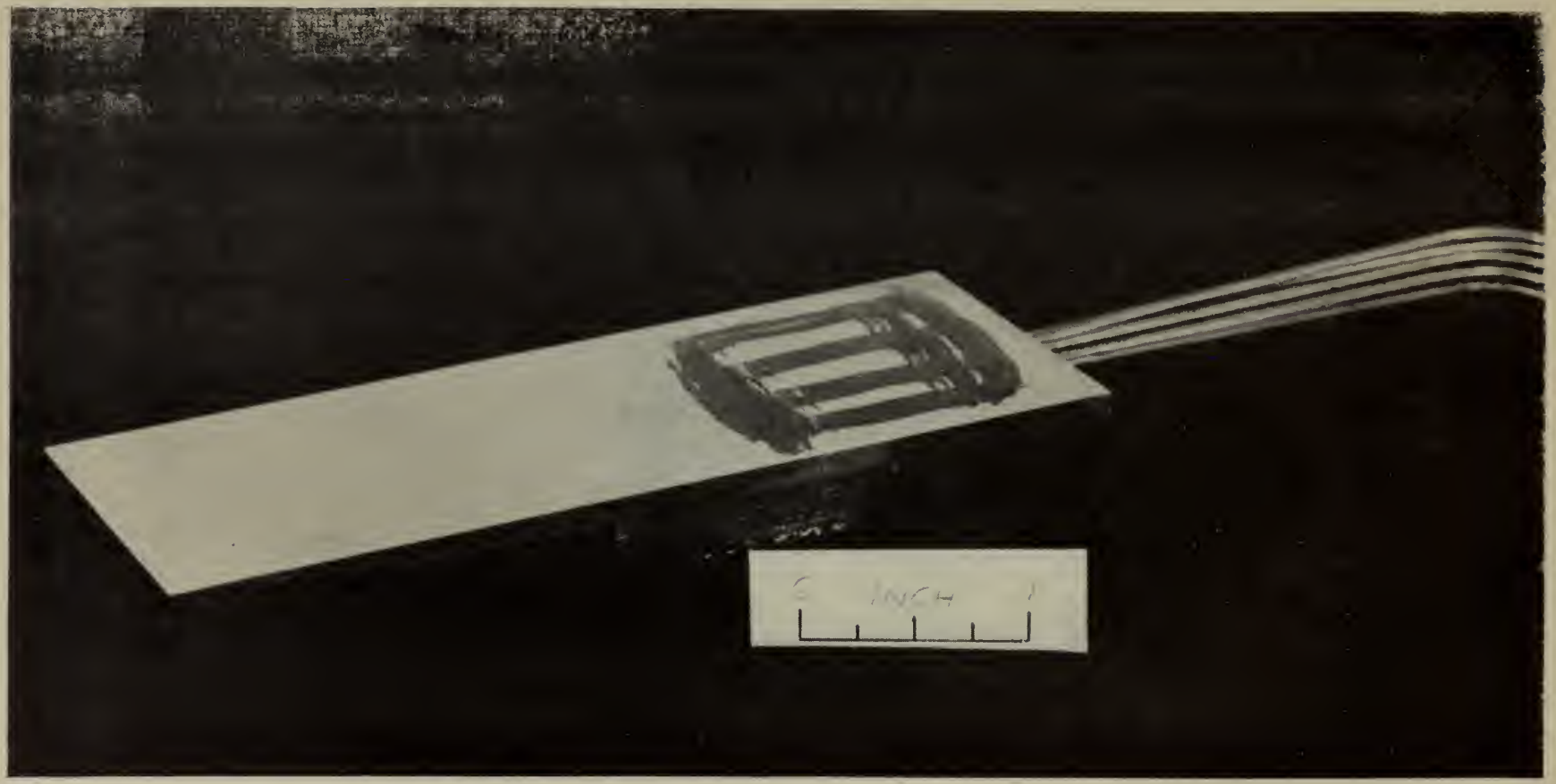

FIG. 1B C

PHOTOGRAPH

OF FLAT PLATE

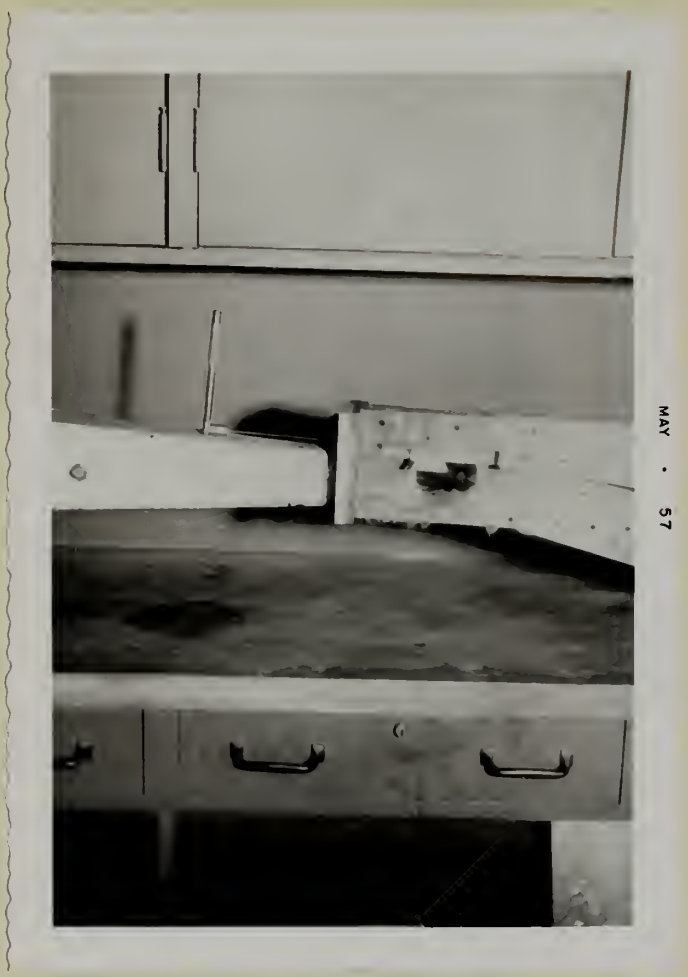

Fig. 1D

RATCHET WRENCH AND

LEAD SCREW MECHANISM

FIG. 2A

5° WEDGE; 10° WEDGE WITH PYLON

LEADING EDGES POINT TO LEFT

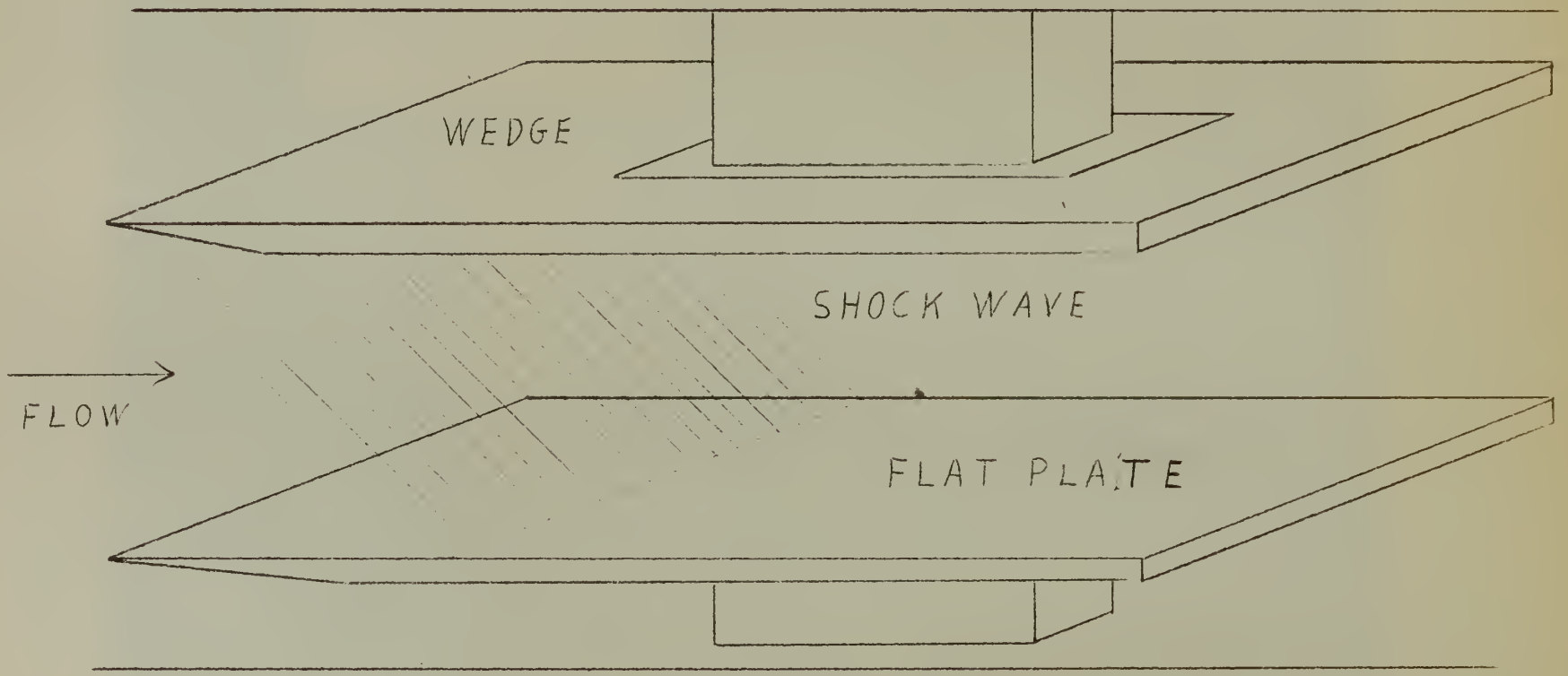

FIG 2B
DRAWING OF FLAT PLATE
WEDGE AND SHOCK WAVE

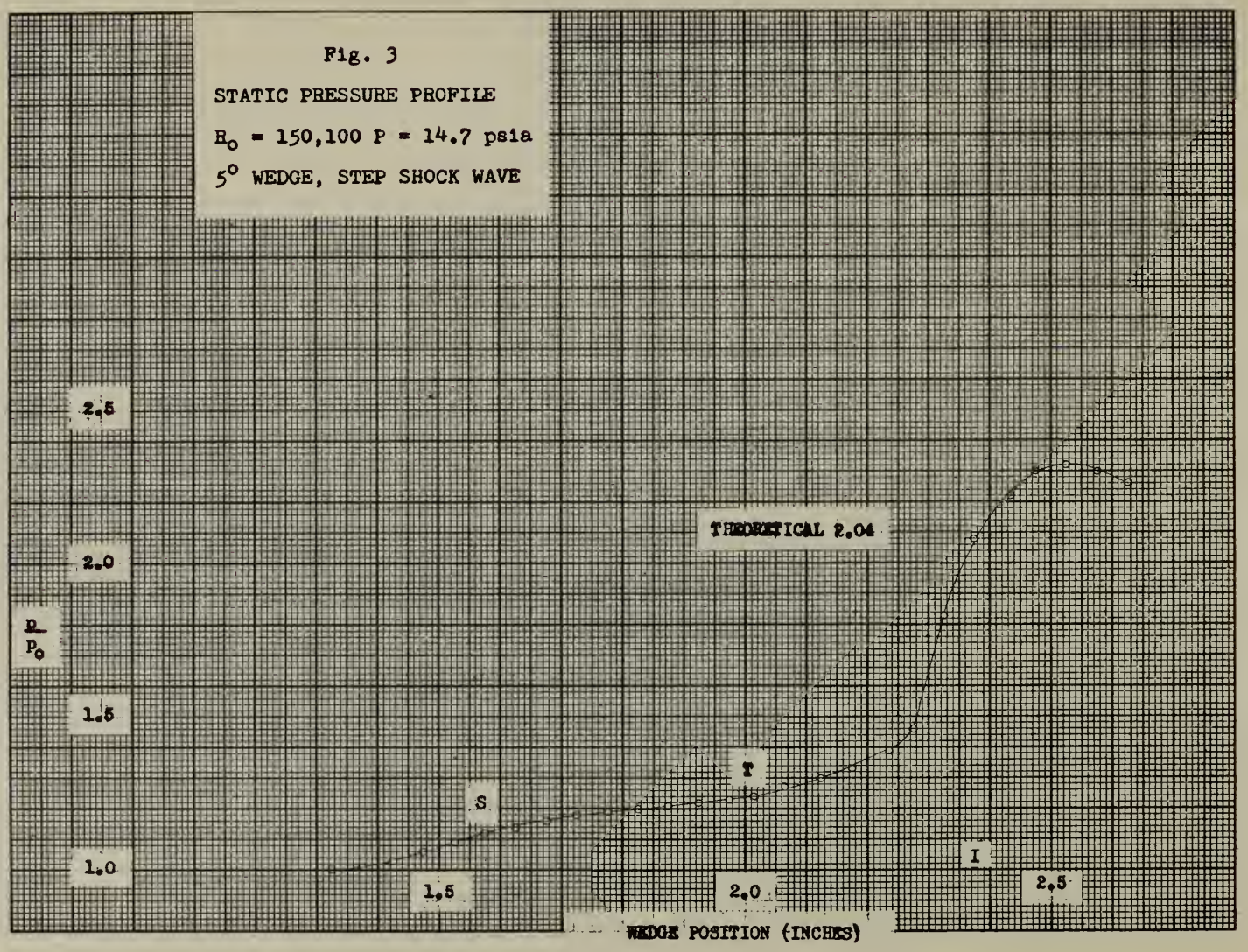
Fig. 3
STATIC PRESSURE PROFILE
R_o = 150,100 P = 14.7 psia
5° WEDGE, STEP SHOCK WAVE
2.5
2.0
$\frac{p}{p_o}$
1.5
1.0
THEORETICAL 2.04
T
S
I
1.5
2.0
2.5
WEDGE POSITION (INCHES)

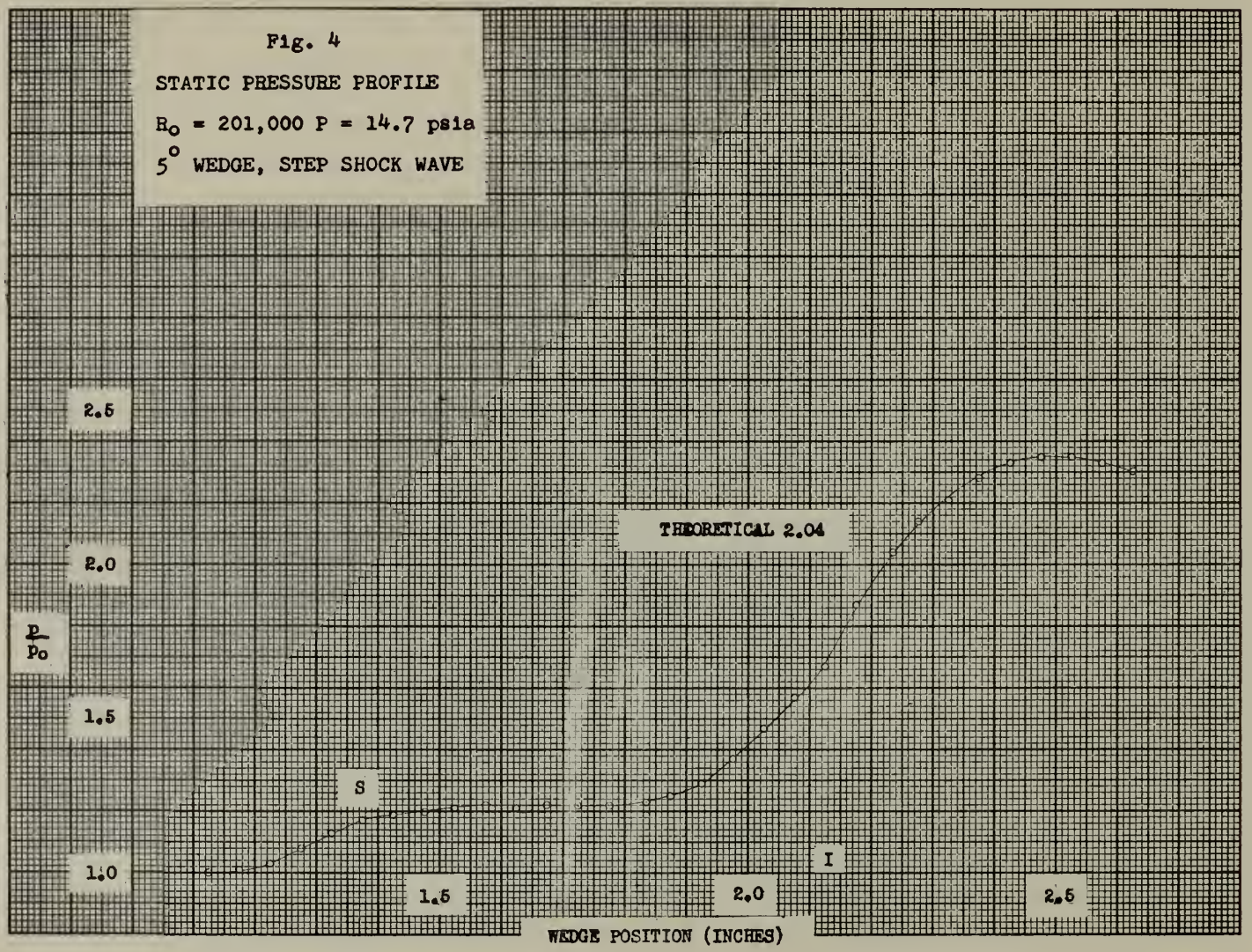
Fig. 4
STATIC PRESSURE PROFILE
R_o = 201,000 P = 14.7 psia
5° WEDGE, STEP SHOCK WAVE
2.5
2.0
1.5
1.0
$\frac{p}{p_o}$
THEORETICAL 2.04
S
I
1.5
2.0
2.5
WEDGE POSITION (INCHES)

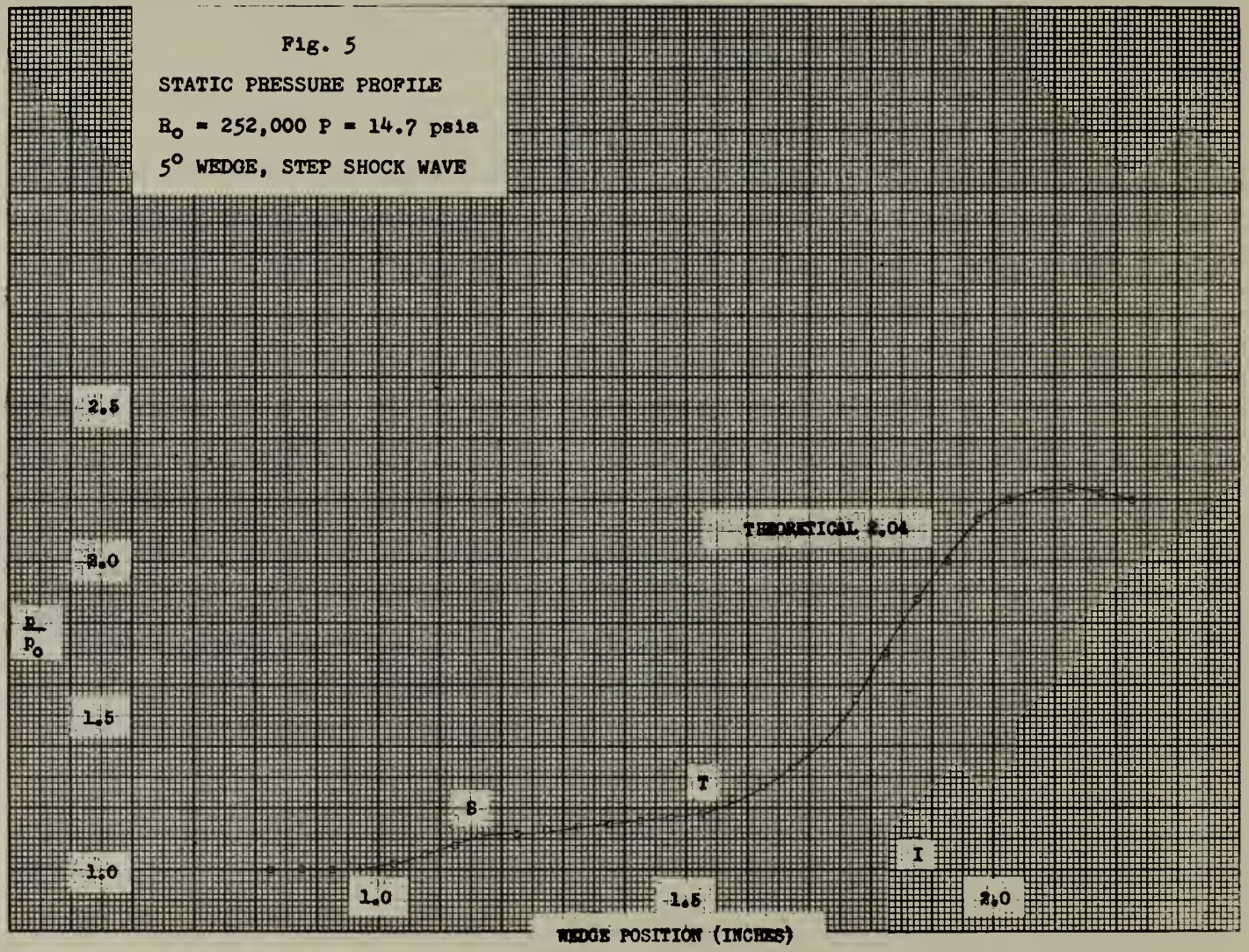
Fig. 5
STATIC PRESSURE PROFILE
R_o = 252,000 P = 14.7 psia
5° WEDGE, STEP SHOCK WAVE
2.5
2.0
$\frac{p}{p_o}$
1.5
1.0
THEORETICAL 2.04
T
S
I
1.0
1.5
2.0
WEDGE POSITION (INCHES)

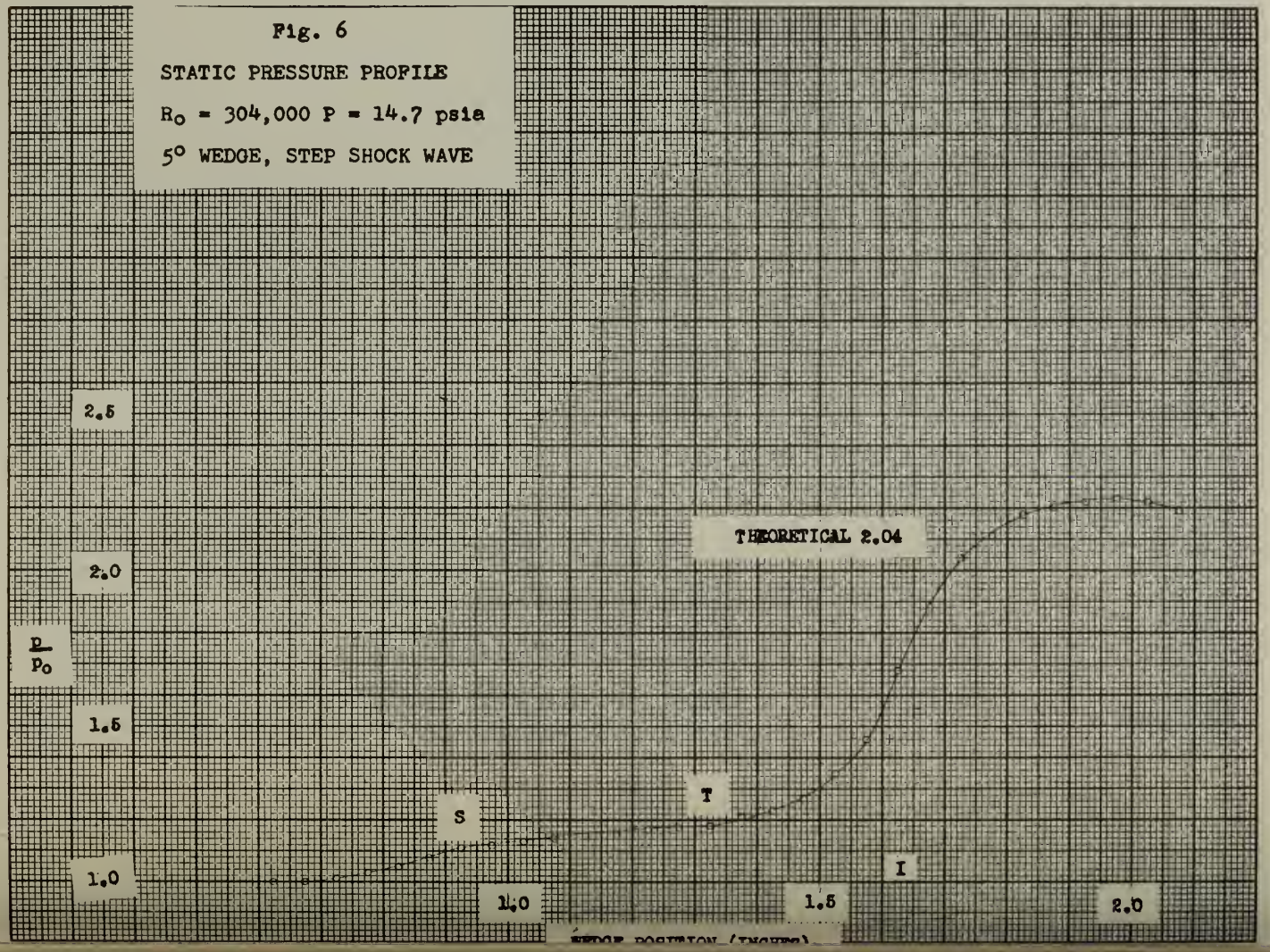
Fig. 6
STATIC PRESSURE PROFILE
R_o = 304,000 P = 14.7 psia
5° WEDGE, STEP SHOCK WAVE
2.5
2.0
$\frac{p}{p_o}$
1.5
1.0
THEORETICAL 2.04
T
S
I
1.0
1.5
2.0

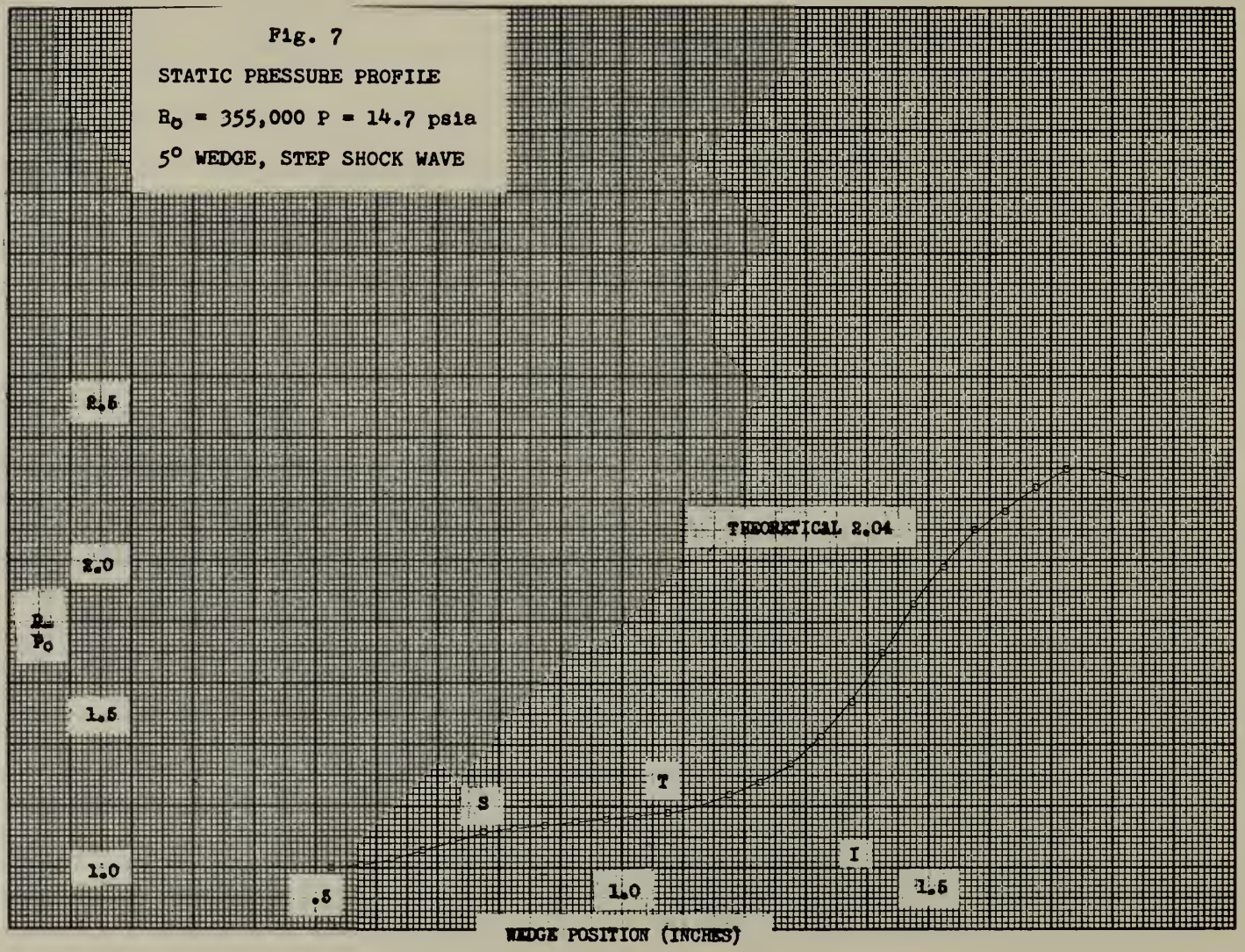
Fig. 7
STATIC PRESSURE PROFILE
R_o = 355,000 P = 14.7 psia
5° WEDGE, STEP SHOCK WAVE
2.5
2.0
$\frac{P}{P_o}$
1.5
1.0
.5
1.0
1.5
S
T
I
THEORETICAL 2.04
WEDGE POSITION (INCHES)

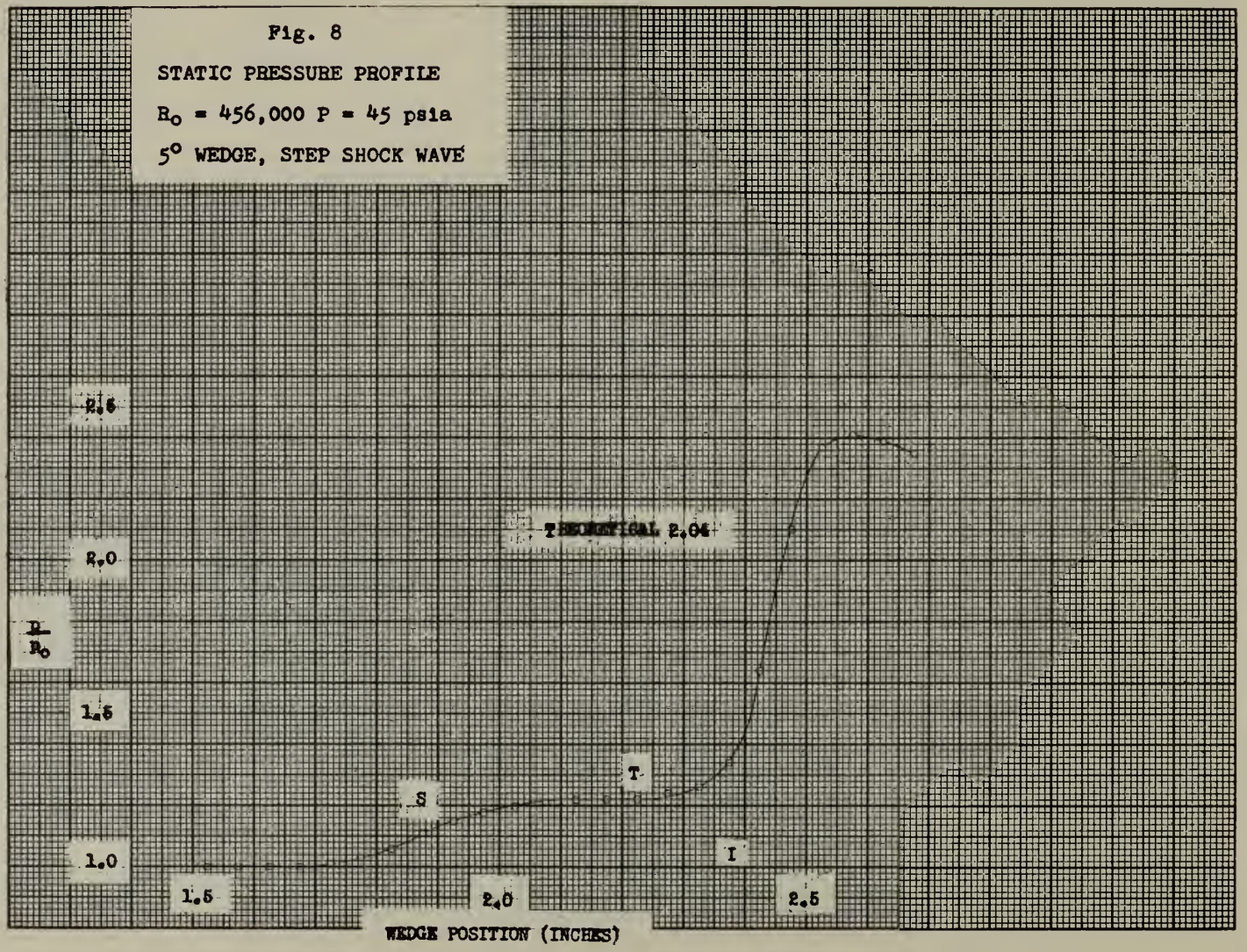
Fig. 8
STATIC PRESSURE PROFILE
R_o = 456,000 P = 45 psia
5° WEDGE, STEP SHOCK WAVE
2.5
THEORETICAL 2.04
2.0
P/P_o
1.5
T
S
1.0
I
1.5
2.0
2.5
WEDGE POSITION (INCHES)

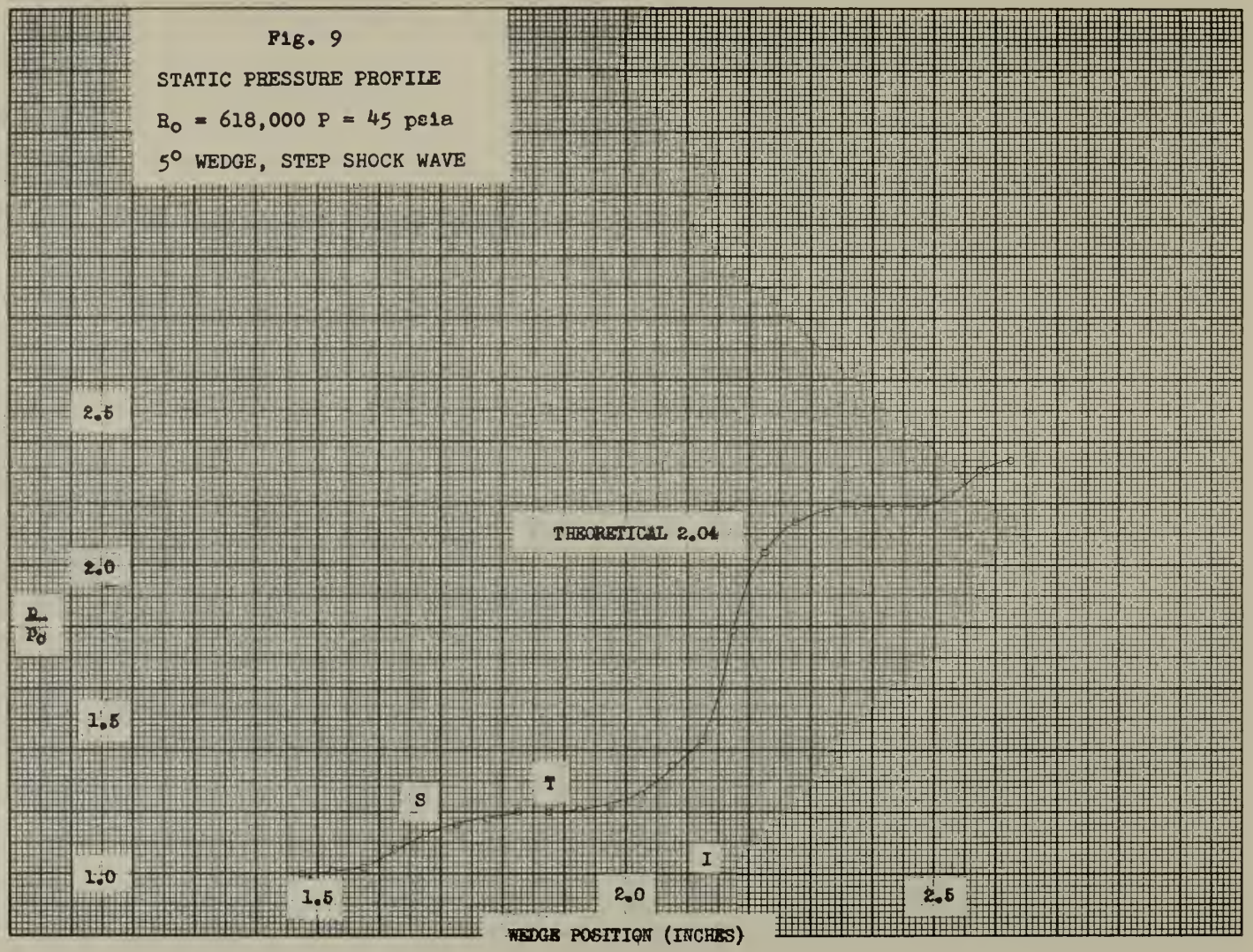
Fig. 9
STATIC PRESSURE PROFILE
R_o = 618,000 P = 45 psia
5° WEDGE, STEP SHOCK WAVE
2.5
2.0
$\frac{P_2}{P_0}$
1.5
1.0
THEORETICAL 2.04
S
T
I
1.5
2.0
2.5
WEDGE POSITION (INCHES)

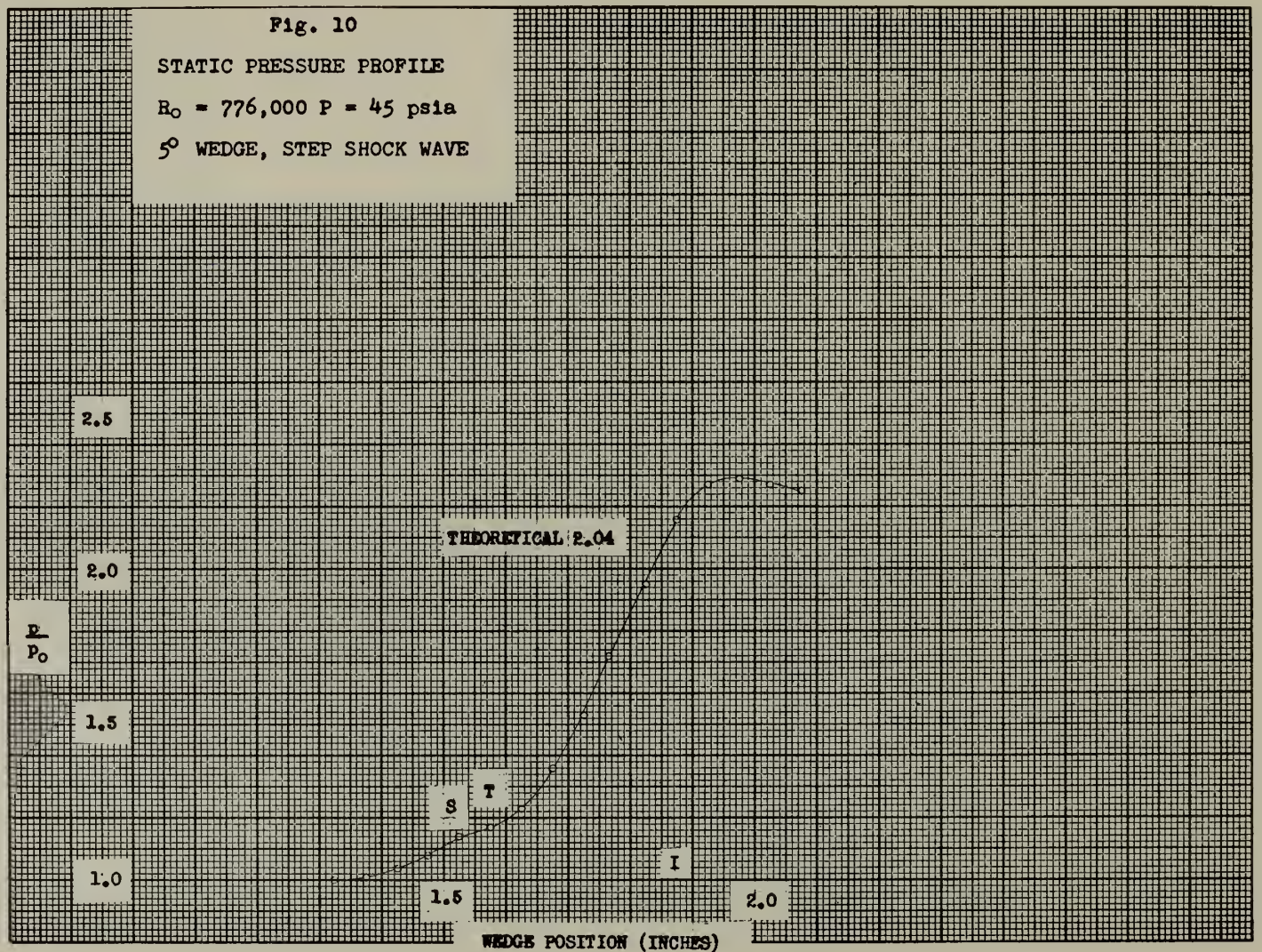
Fig. 10
STATIC PRESSURE PROFILE
R_o = 776,000 P = 45 psia
5° WEDGE, STEP SHOCK WAVE
2.5
2.0
$\frac{P}{P_o}$
1.5
1.0
THEORETICAL 2.04
S
T
I
1.5
2.0
WEDGE POSITION (INCHES)

Fig. 11

STATIC PRESSURE PROFILE

R_o = 936,000 P = 45 psia

5° WEDGE, STEP SHOCK WAVE

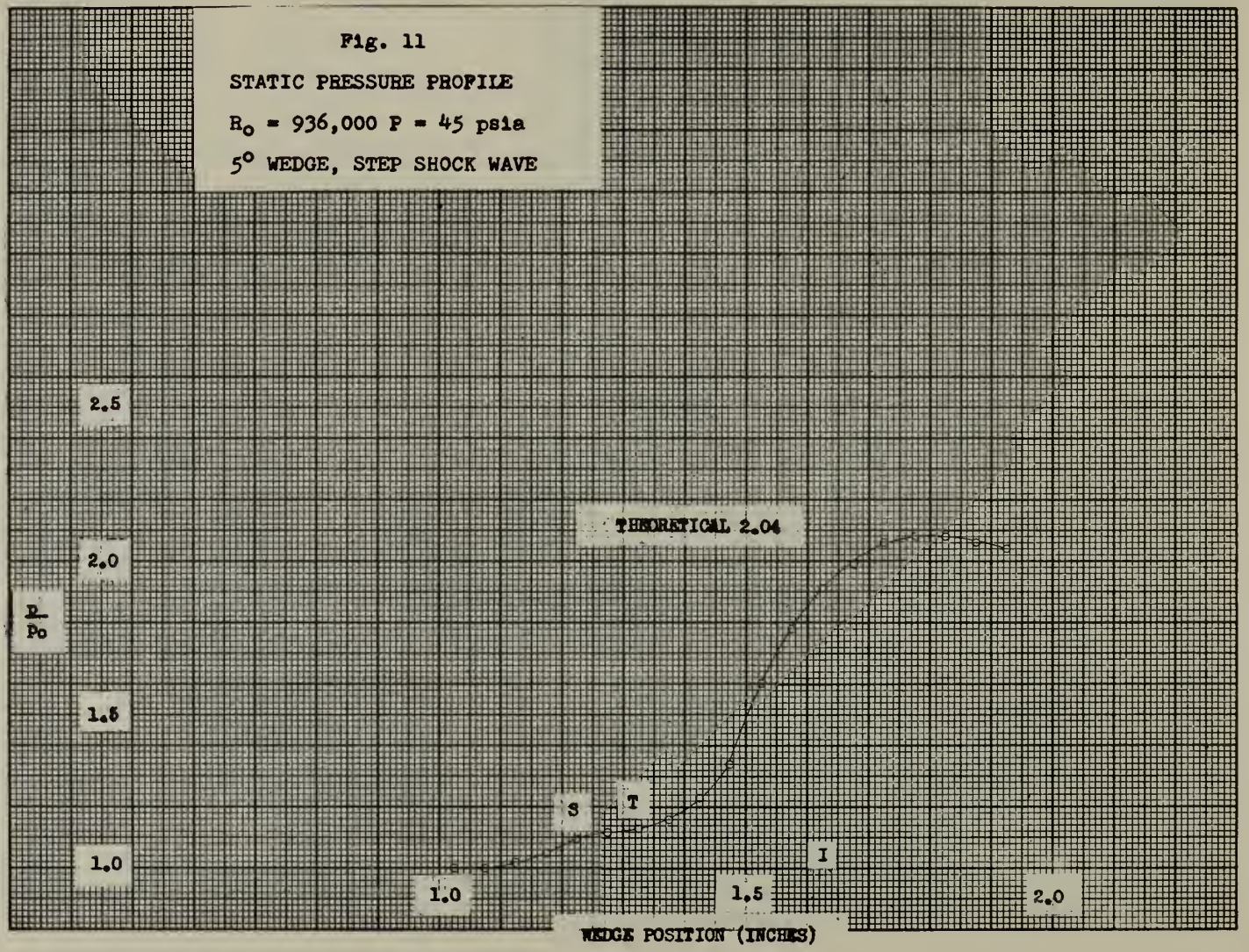

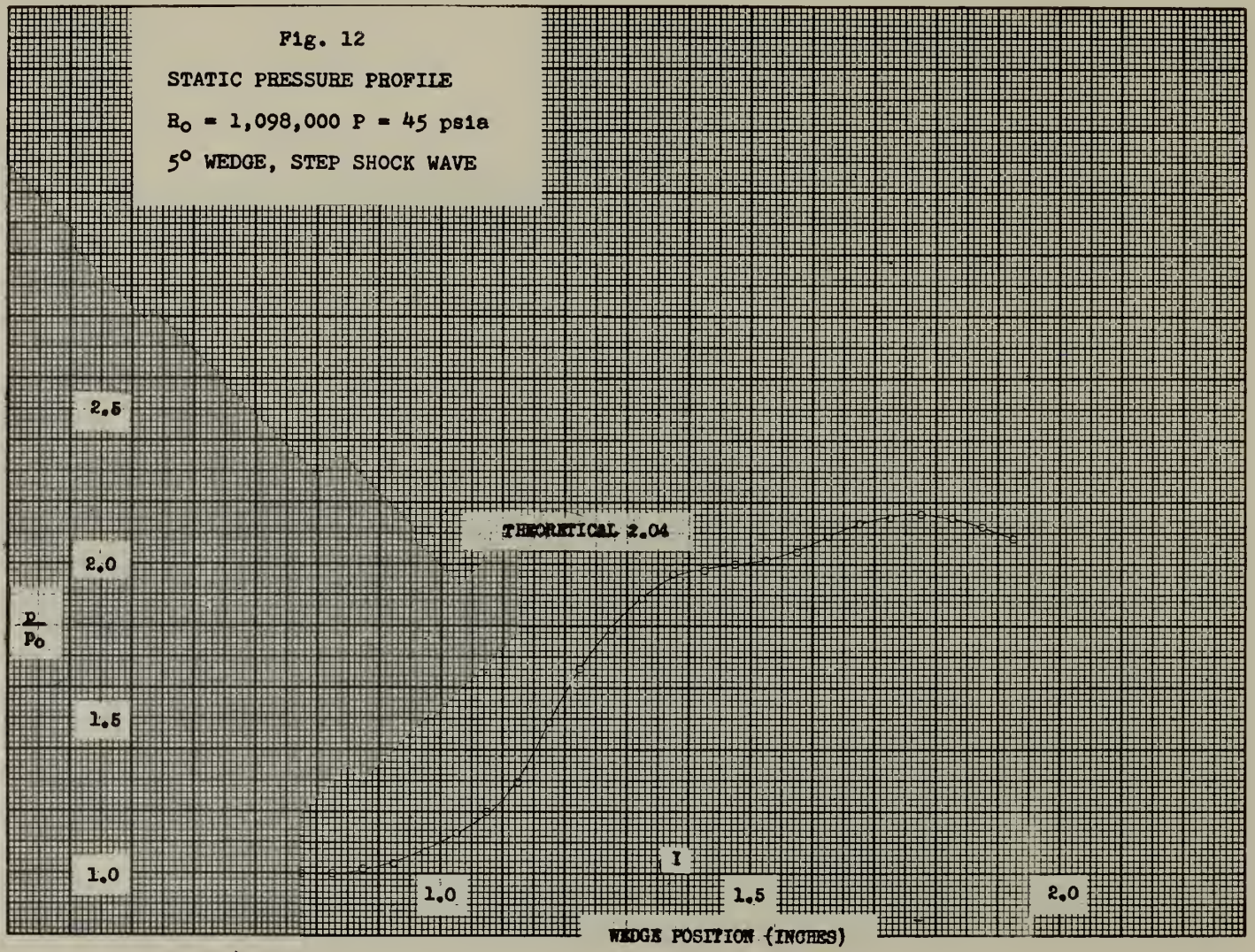
Fig. 12
STATIC PRESSURE PROFILE
R_o = 1,098,000 P = 45 psia
5° WEDGE, STEP SHOCK WAVE
2.5
2.0
$\frac{p}{p_o}$
1.5
1.0
THEORETICAL 2.04
I
1.0
1.5
2.0
WEDGE POSITION (INCHES)

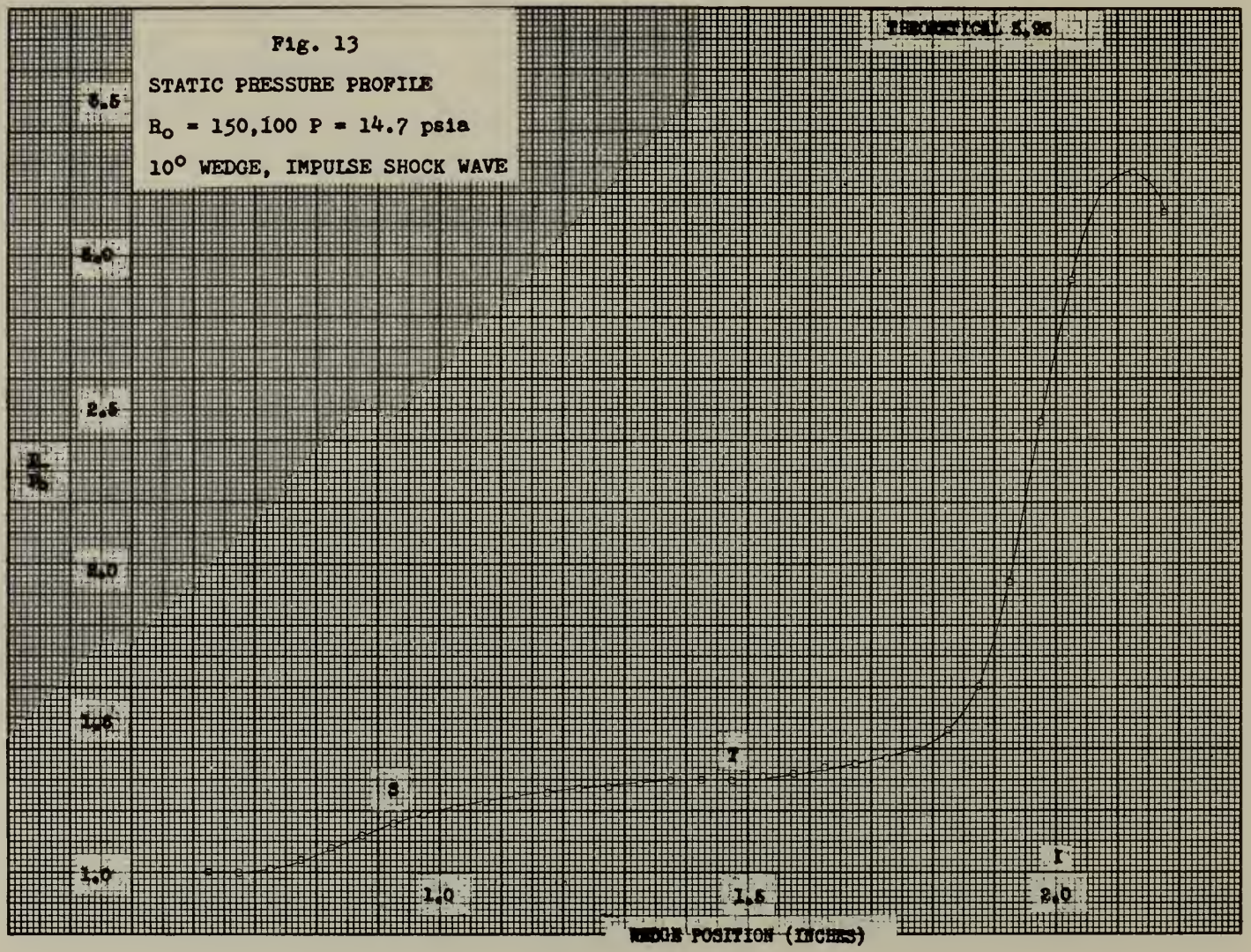
Fig. 13
STATIC PRESSURE PROFILE
R_o = 150,100 P = 14.7 psia
10° WEDGE, IMPULSE SHOCK WAVE
THEORETICAL 5.96
3.5
3.0
2.5
2.0
1.5
1.0
3
2
1
1.0
1.5
2.0
WEDGE POSITION (INCHES)

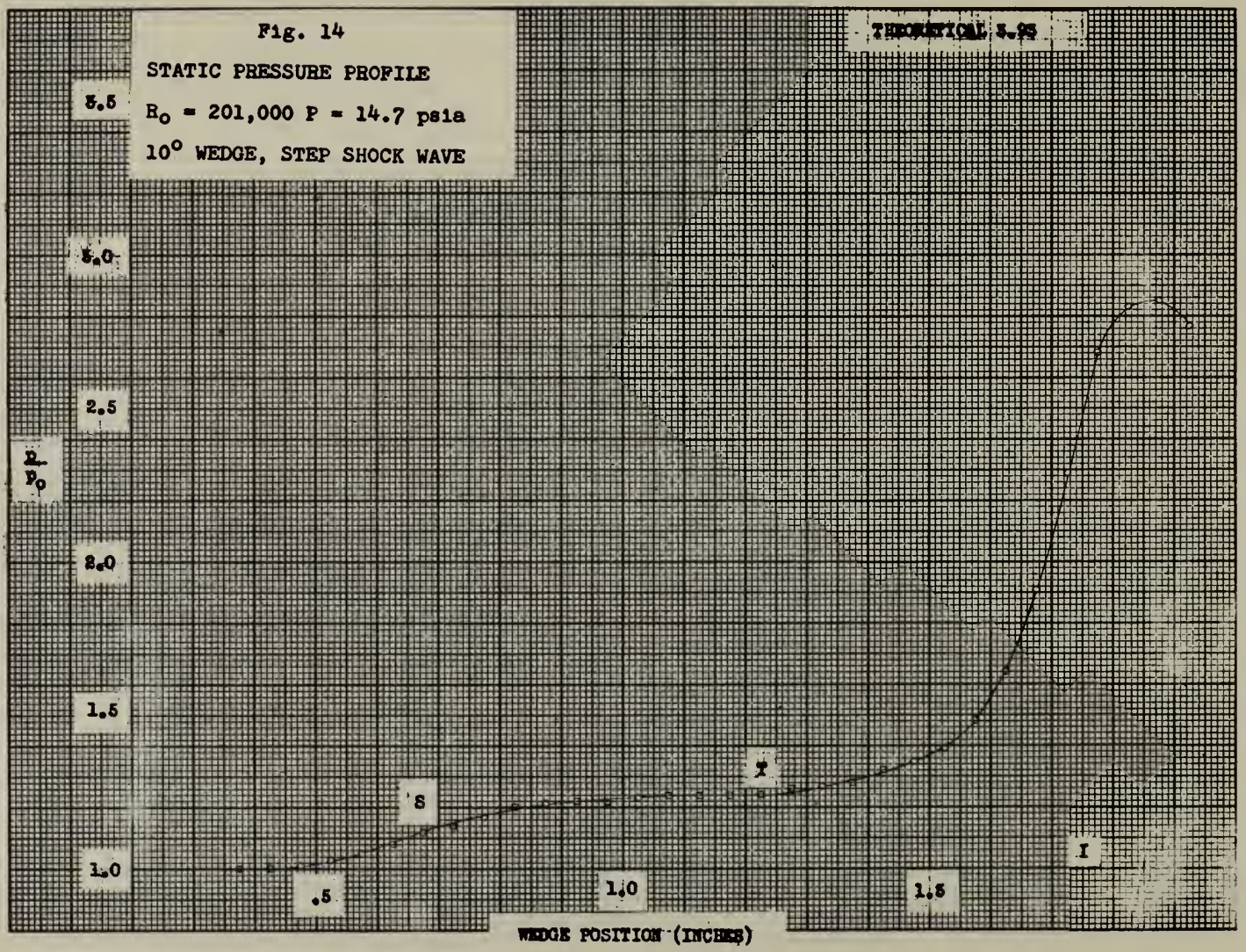
Fig. 14
STATIC PRESSURE PROFILE
R_o = 201,000 P = 14.7 psia
10° WEDGE, STEP SHOCK WAVE
THEORETICAL 3.25
3.5
3.0
2.5
$\frac{p}{p_o}$
2.0
1.5
1.0
S
I
.5
1.0
1.5
WEDGE POSITION (INCHES)

Fig. 15

STATIC PRESSURE PROFILE

R_o = 252,000 P = 14.7 psia

10° WEDGE, IMPULSE SHOCK WAVE

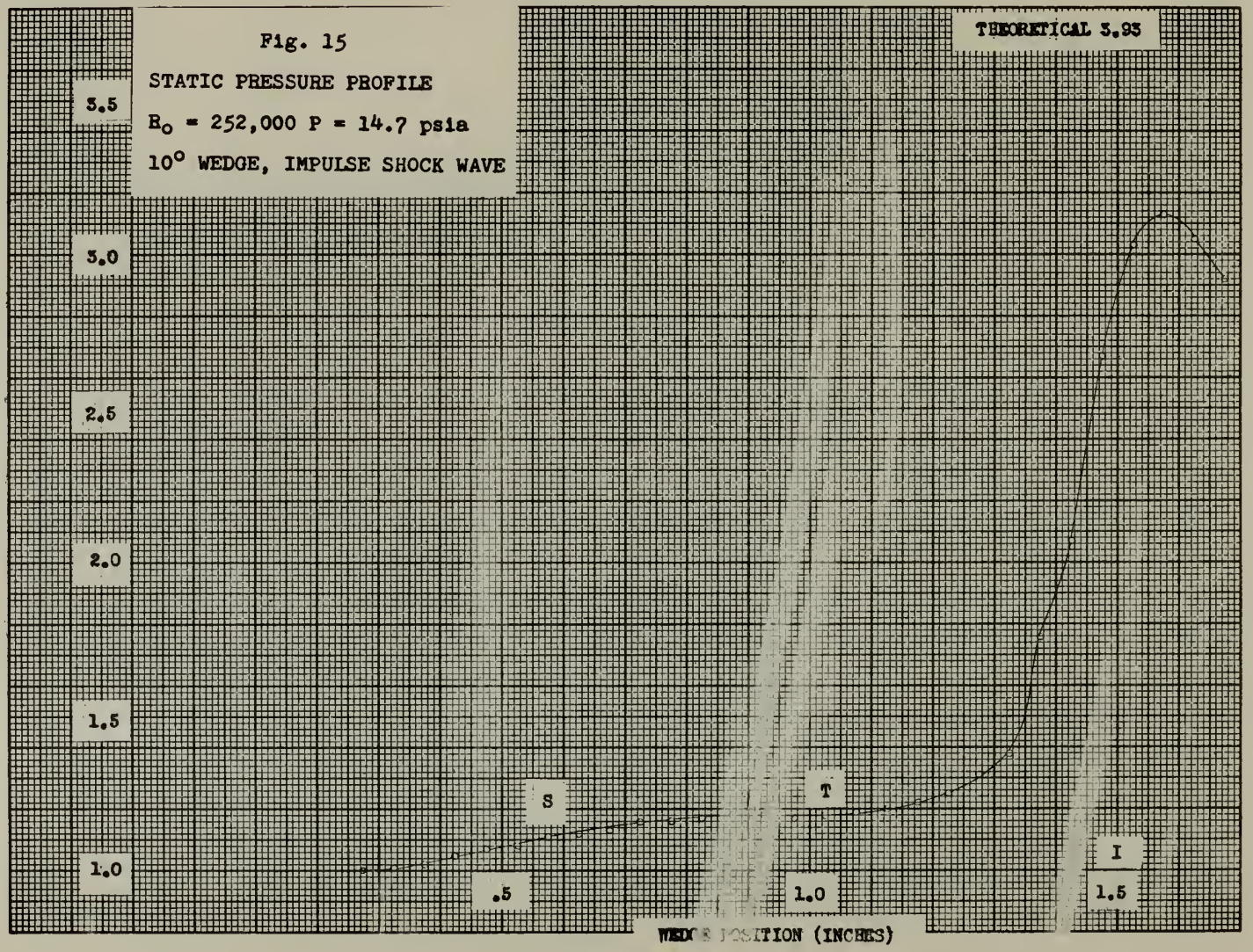

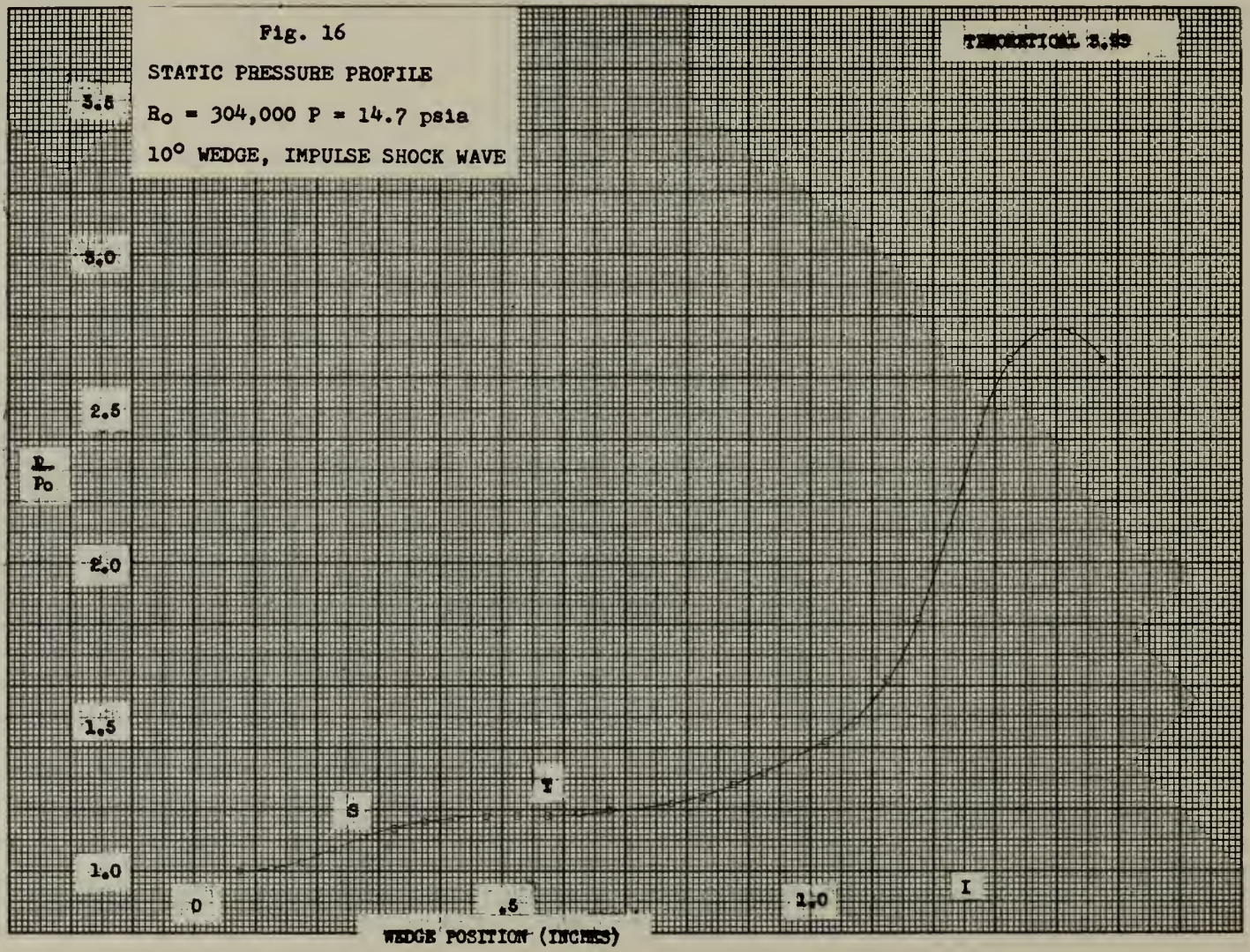
Fig. 16
STATIC PRESSURE PROFILE
R_o = 304,000 P = 14.7 psia
10° WEDGE, IMPULSE SHOCK WAVE
3.5
3.0
2.5
P/Po
2.0
1.5
1.0
0
.5
1.0
S
T
I
WEDGE POSITION (INCHES)

Fig. 17(a)

STATIC PRESSURE PROFILE

R_o = 355,000 P = 14.7 psia

10° WEDGE, IMPULSE SHOCK WAVE

Fig. 17(b)

STATIC PRESSURE PROFILE

10° WEDGE, IMPULSE SHOCK WAVE
SHORTENED HORIZONTAL SCALE
EXTENDED PROFILE BEYOND
PRESSURE PEAK

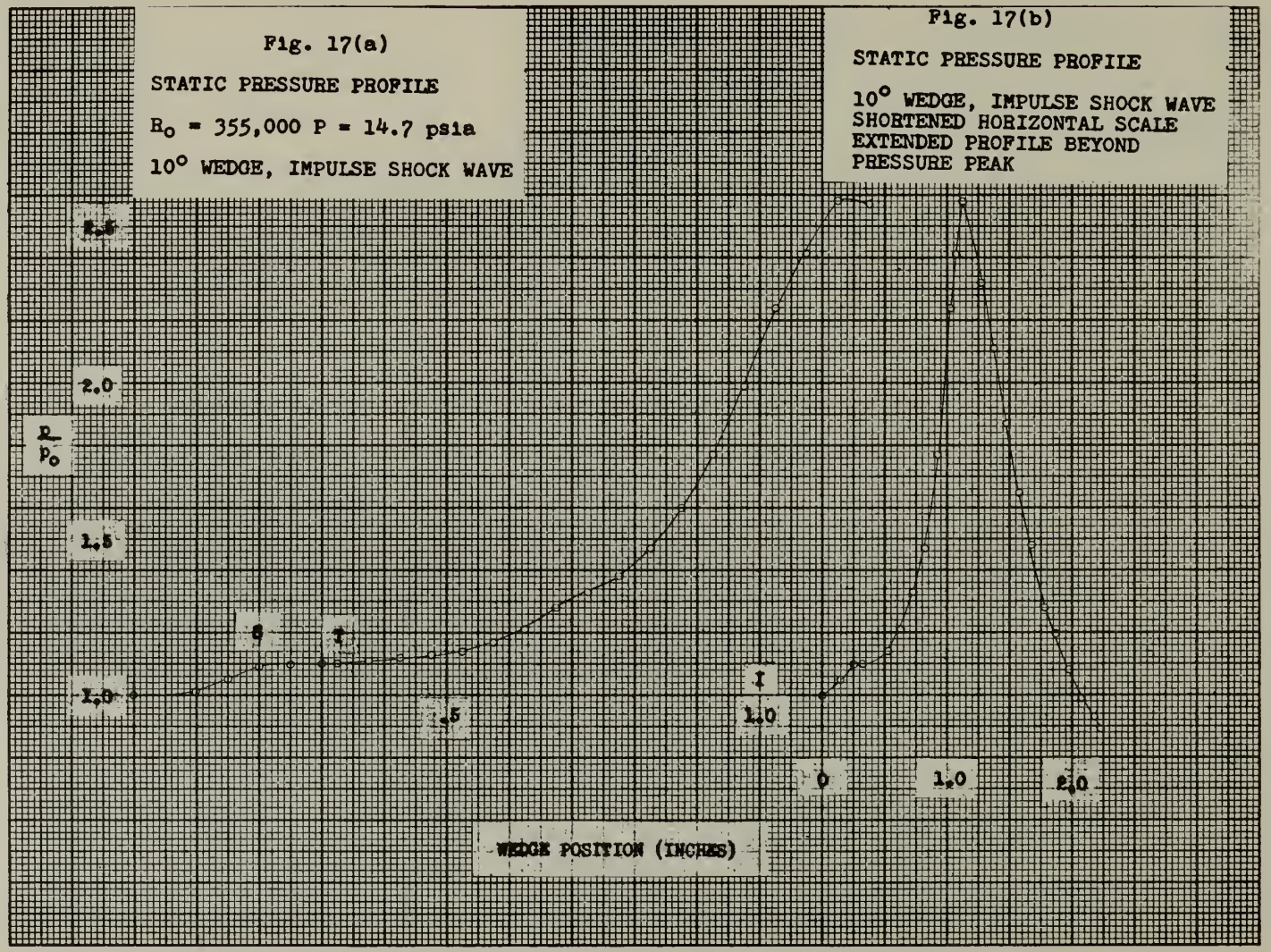

Fig. 18

STATIC PRESSURE PROFILE

R_o = 456,000 P = 45 psia

10° WEDGE, IMPULSE SHOCK WAVE

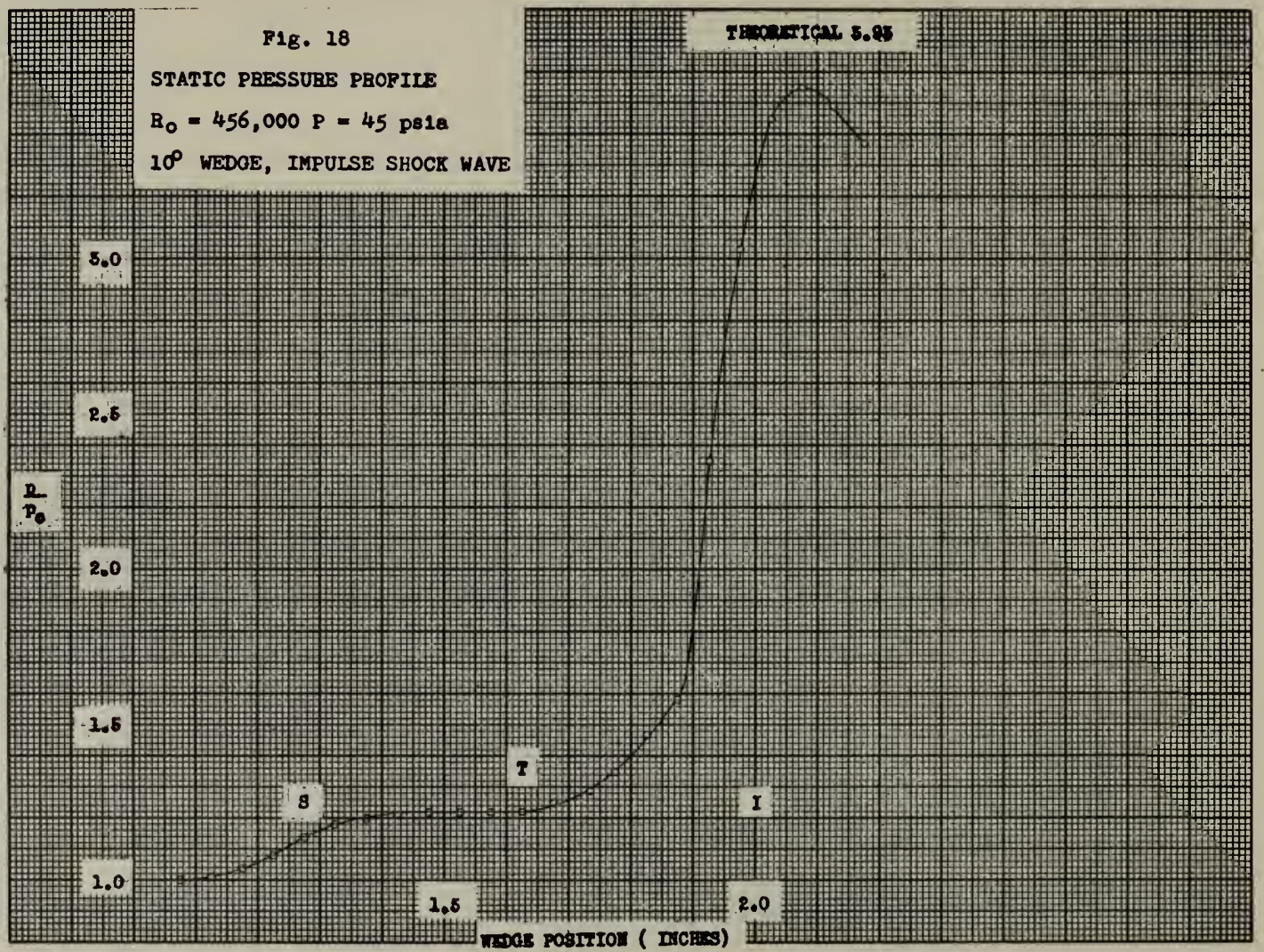

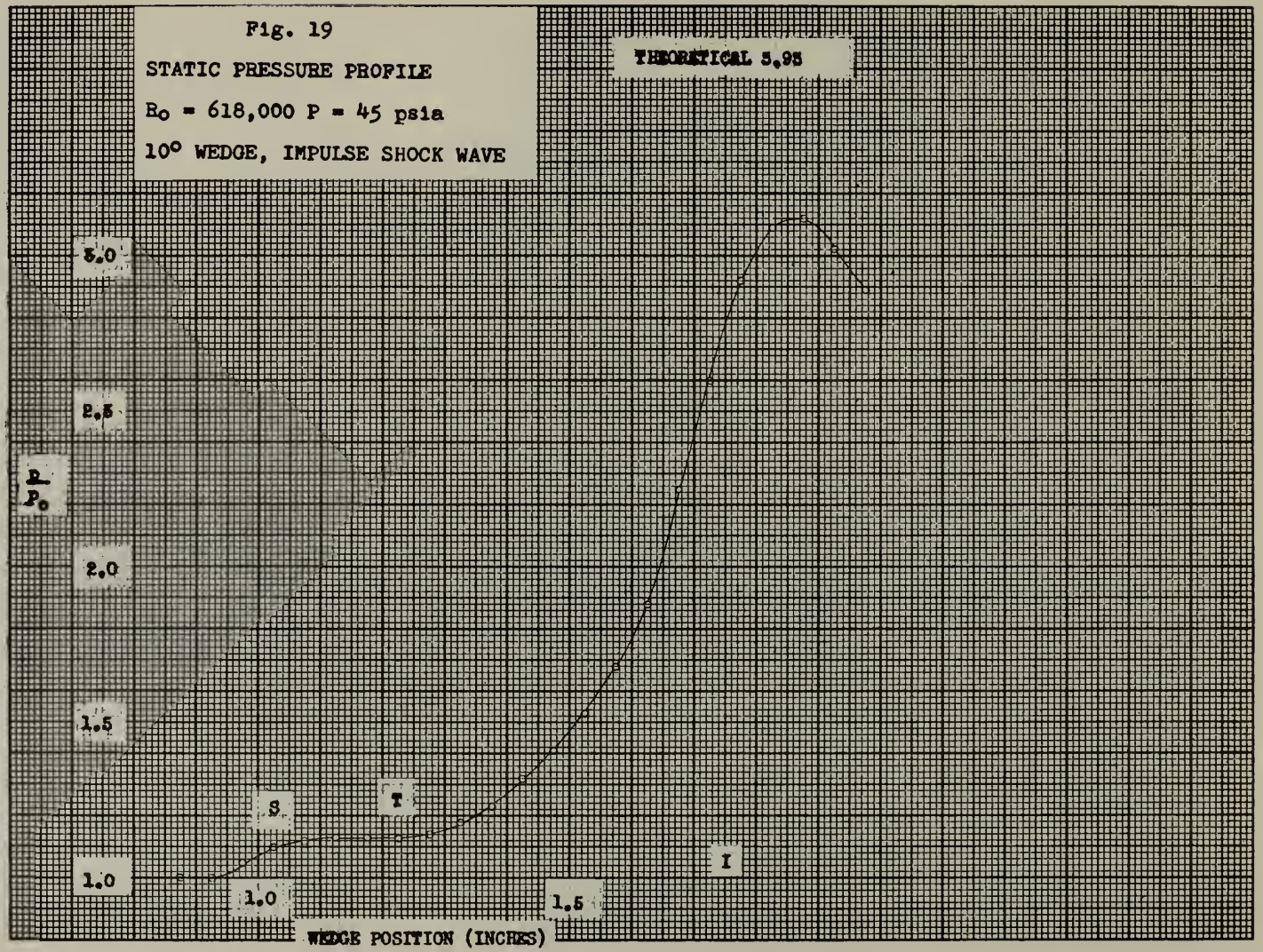
Fig. 19
STATIC PRESSURE PROFILE
R_o = 618,000 P = 45 psia
10° WEDGE, IMPULSE SHOCK WAVE
THEORETICAL 5.95
3.0
2.5
$\frac{P}{P_o}$
2.0
1.5
1.0
S
T
I
1.0
1.5
WEDGE POSITION (INCHES)

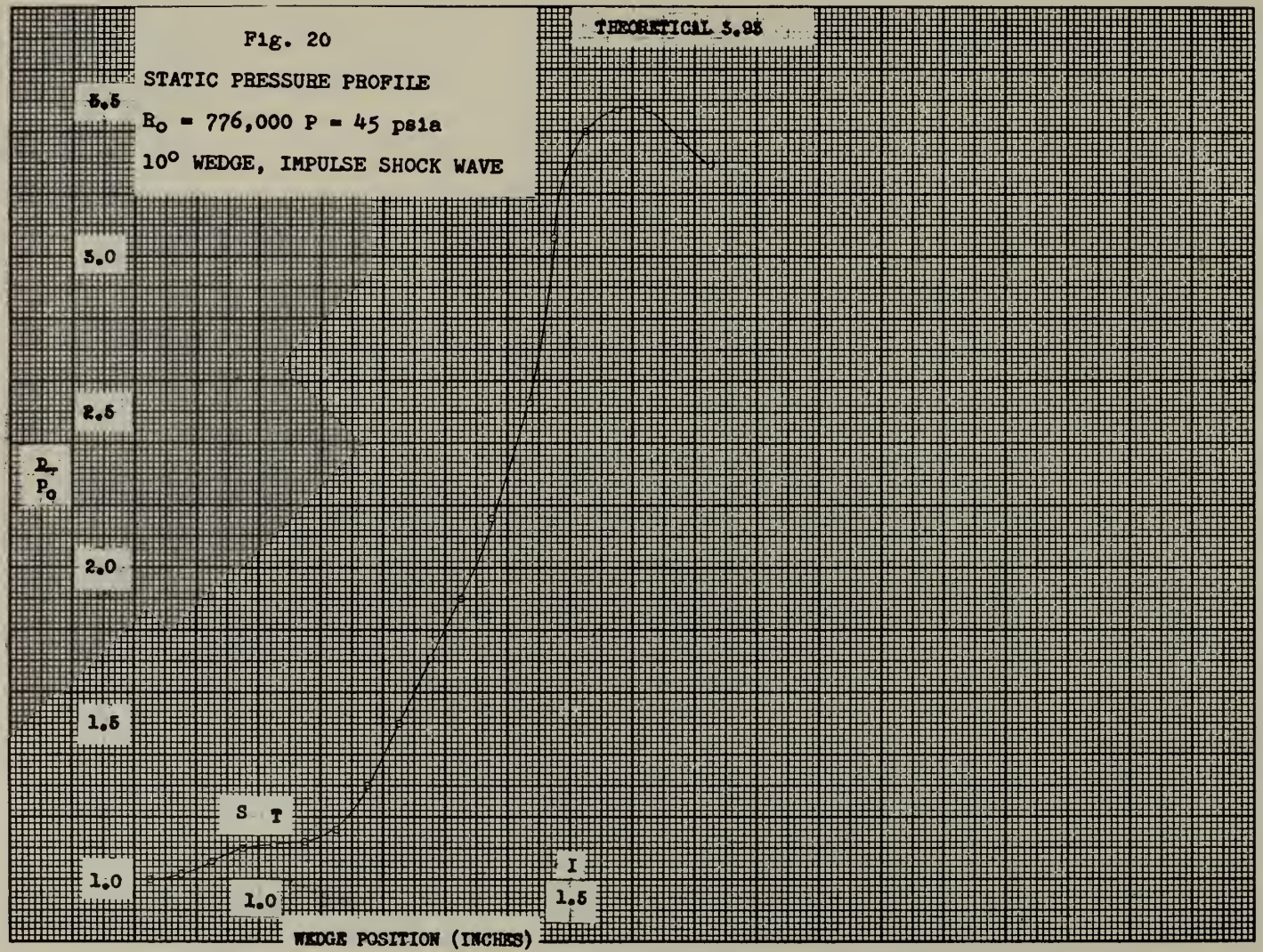
Fig. 20
STATIC PRESSURE PROFILE
R_o = 776,000 P = 45 psia
10° WEDGE, IMPULSE SHOCK WAVE
THEORETICAL 3.98
3.5
3.0
2.5
$\frac{P}{P_o}$
2.0
1.5
1.0
S T
I
1.0
1.5
WEDGE POSITION (INCHES)

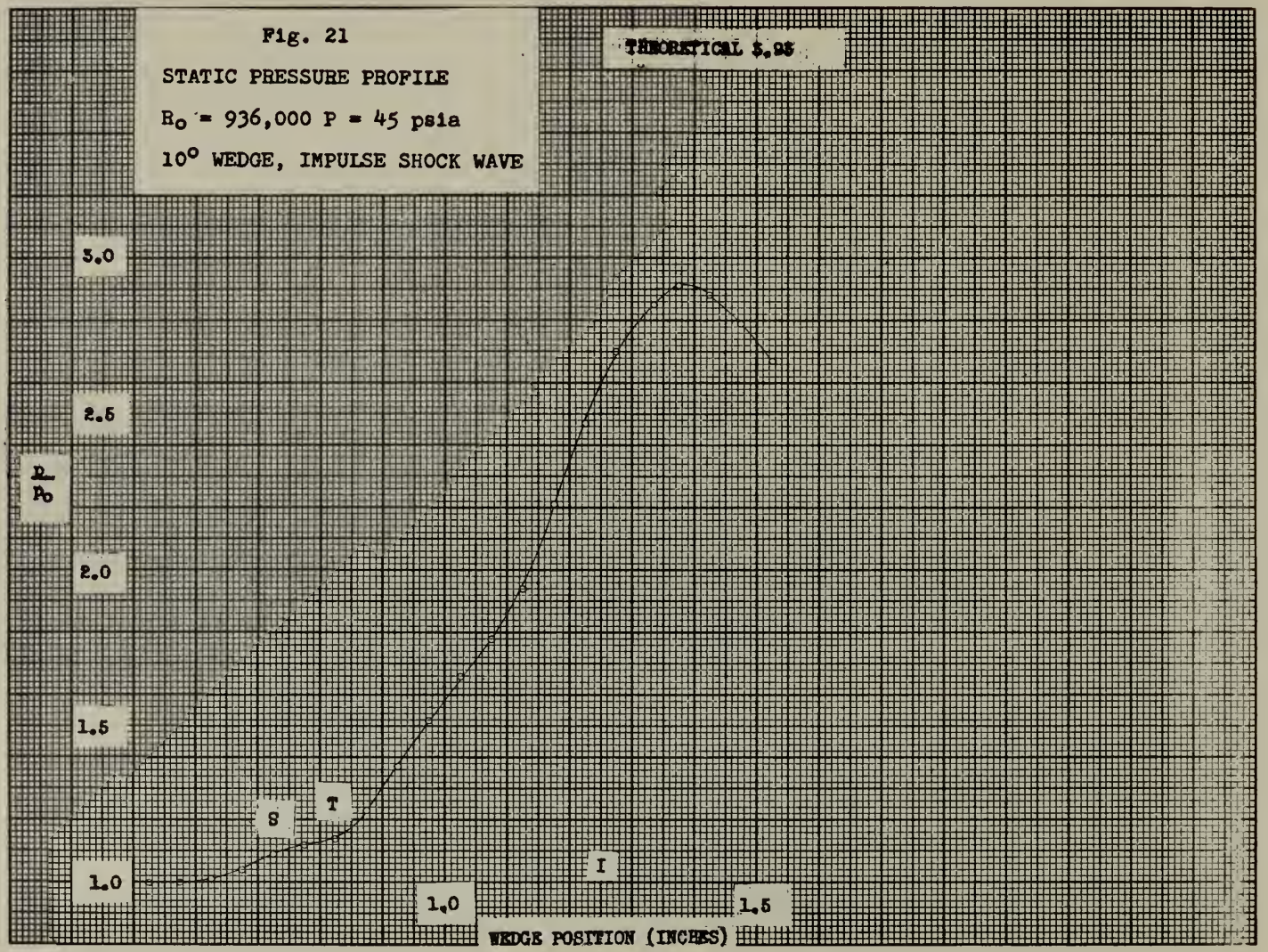
Fig. 21
STATIC PRESSURE PROFILE
R_o = 936,000 P = 45 psia
10° WEDGE, IMPULSE SHOCK WAVE
THEORETICAL δ.95
3.0
2.5
$\frac{P}{P_o}$
2.0
1.5
1.0
S
T
I
1.0
1.5
WEDGE POSITION (INCHES)

Fig. 22

STATIC PRESSURE PROFILE

10° WEDGE, IMPULSE SHOCK WAVE

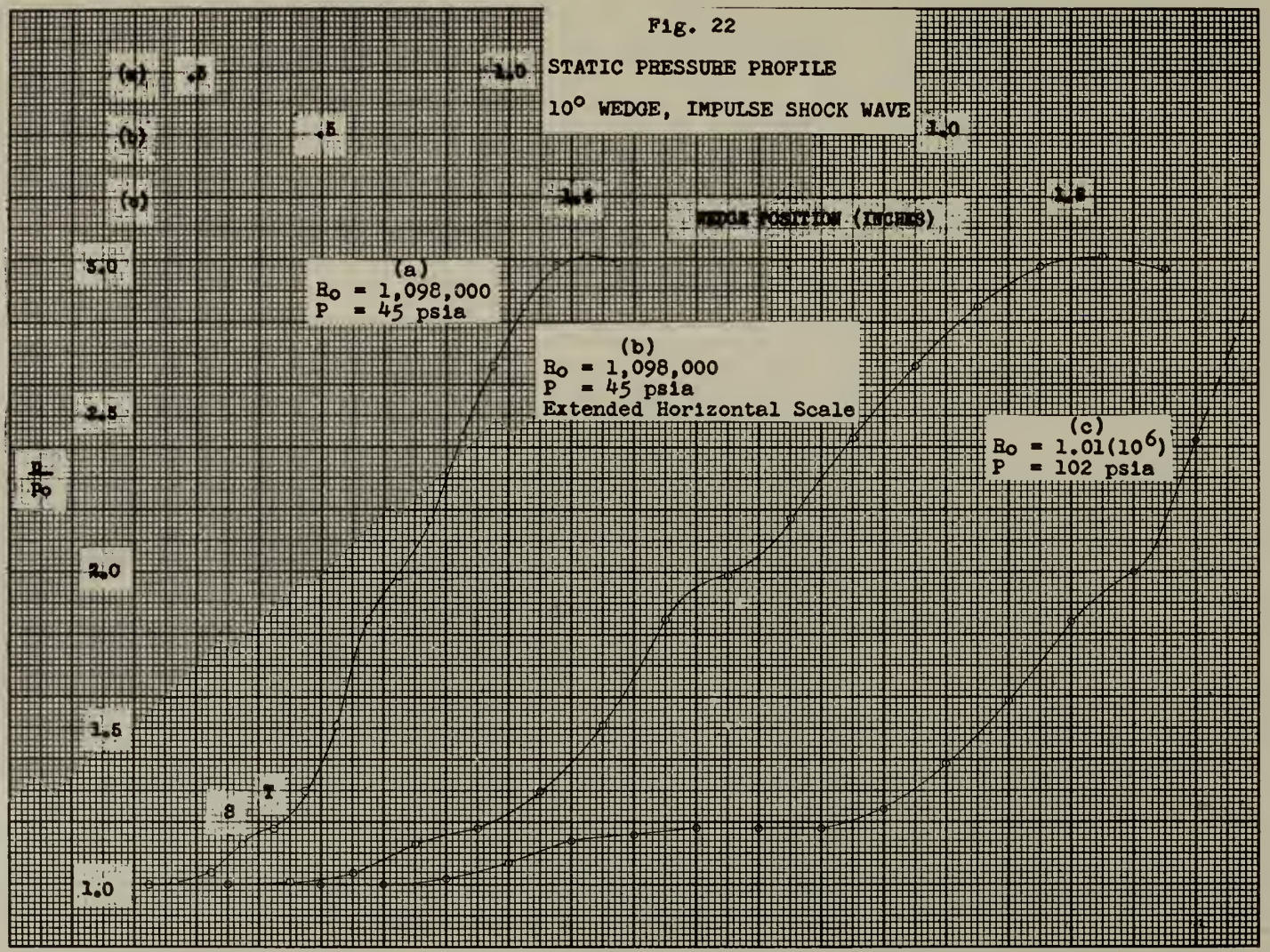

Fig. 23

FACTOR $\frac{d}{\delta_o^*}$ AS FUNCTION OF

REYNOLD'S NUMBER (R_o)

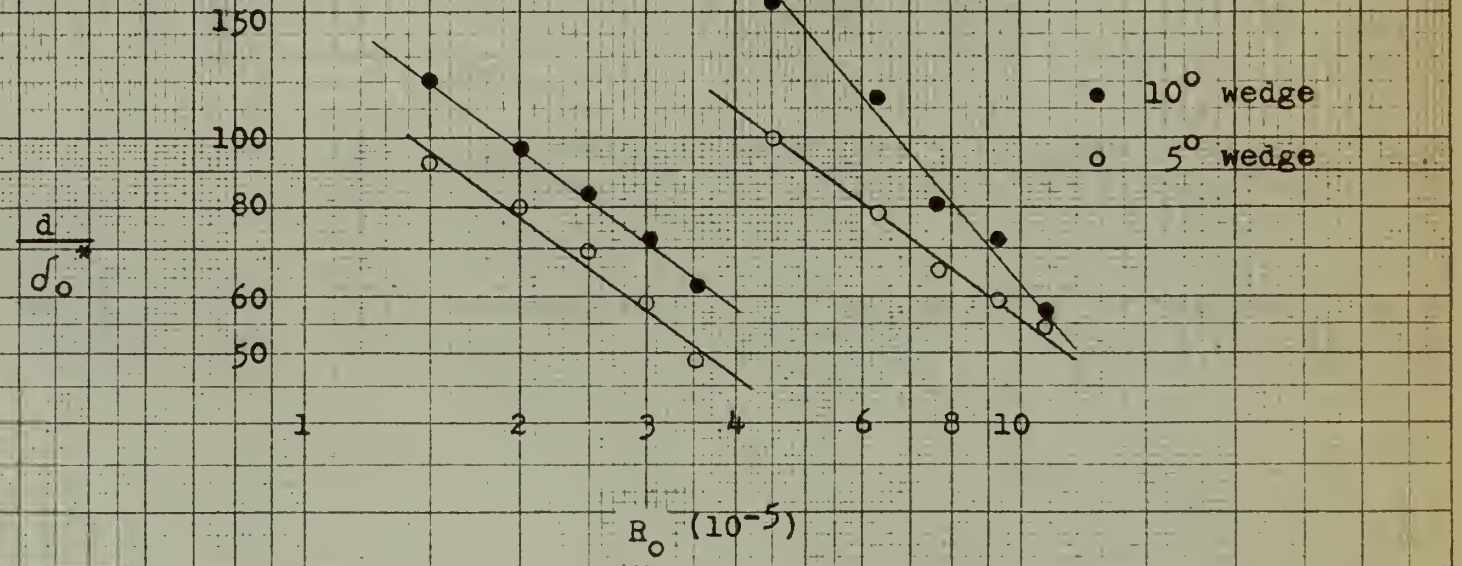

Fig. 24

FACTOR $\frac{d}{\delta_I}$ AS FUNCTION OF REYNOLD'S NUMBER (R_I)

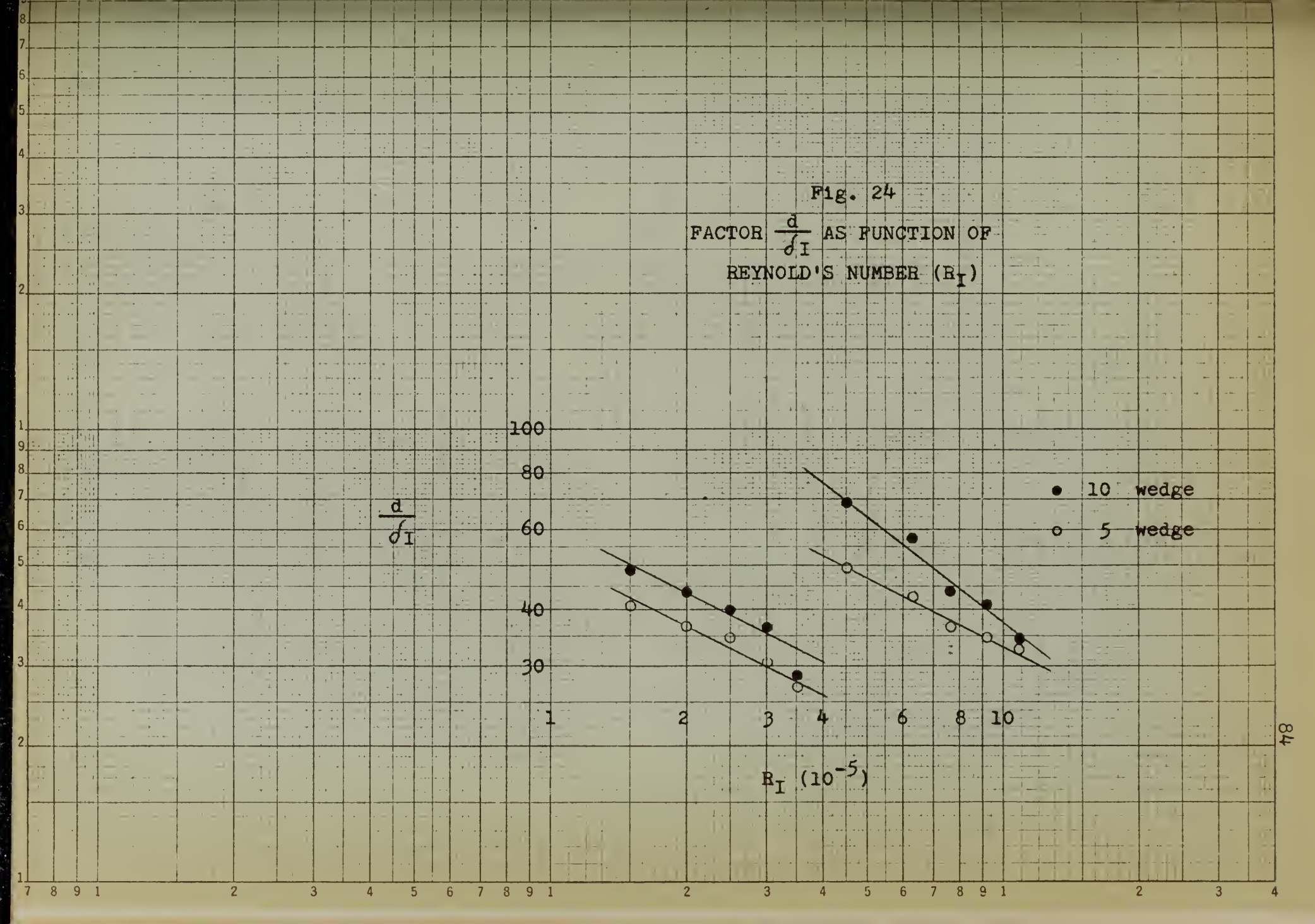

Fig. 25

PRESSURE RATIO AT TOP OF LAMINAR FOOT

versus

REYNOLD'S NUMBER (R_o)

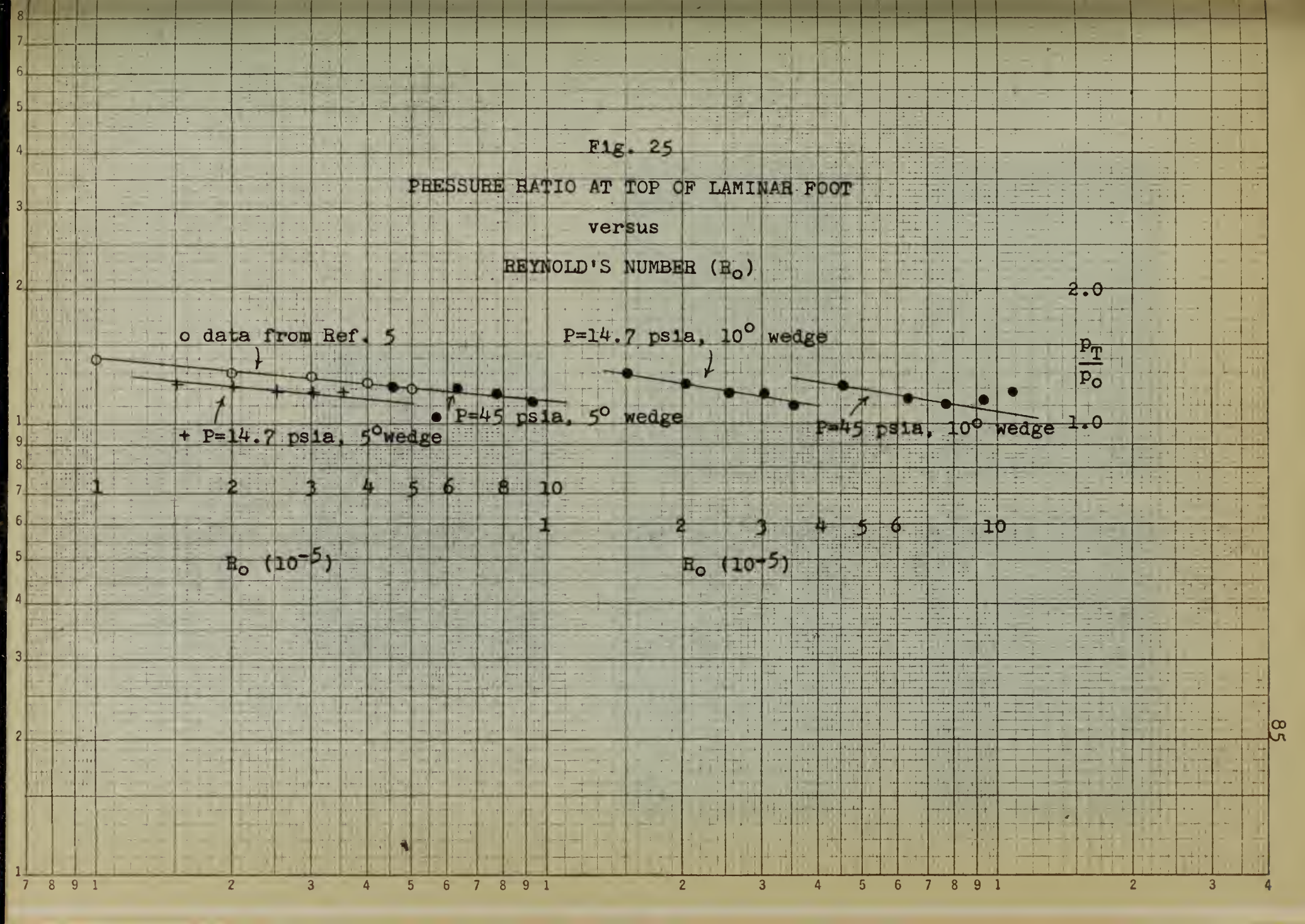

(a) R_I = 150,100

(b) R_I = 201,000

(c) R_I = 252,000

(d) R_I = 315,000

(e) R_I = 355,000

Fig. 26

SHADOW PHOTOGRAPHS

5° WEDGE, P = 14.7 psia

R_I = 150,100 to 355,000

(a) R_I = 776,000

(b) R_I = 936,000

(c) R_I = 1,098,000

Fig. 27

SHADOW PHOTOGRAPHS

5° WEDGE P = 45 psia

R_I = 776,000 to 1,098,000

(a) R_I = 150,100

(b) R_I = 201,000

(c) R_I = 252,000

(d) R_I = 304,000

(e) R_I = 355,000

Fig. 28

SHADOW PHOTOGRAPHS

10^o WEDGE P = 14.7 psia

R_I = 150,100 to 355,000

(a) R_I = 475,500

(b) R_I = 634,000

(c) R_I= 793,000

(d) R_I = 951,000

(e) R_I = 1,098,000

Fig. 29

SHADOW PHOTOGRAPHS

10° WEDGE P = 45 psia

R_I = 475,500 to 1,0[illegible]

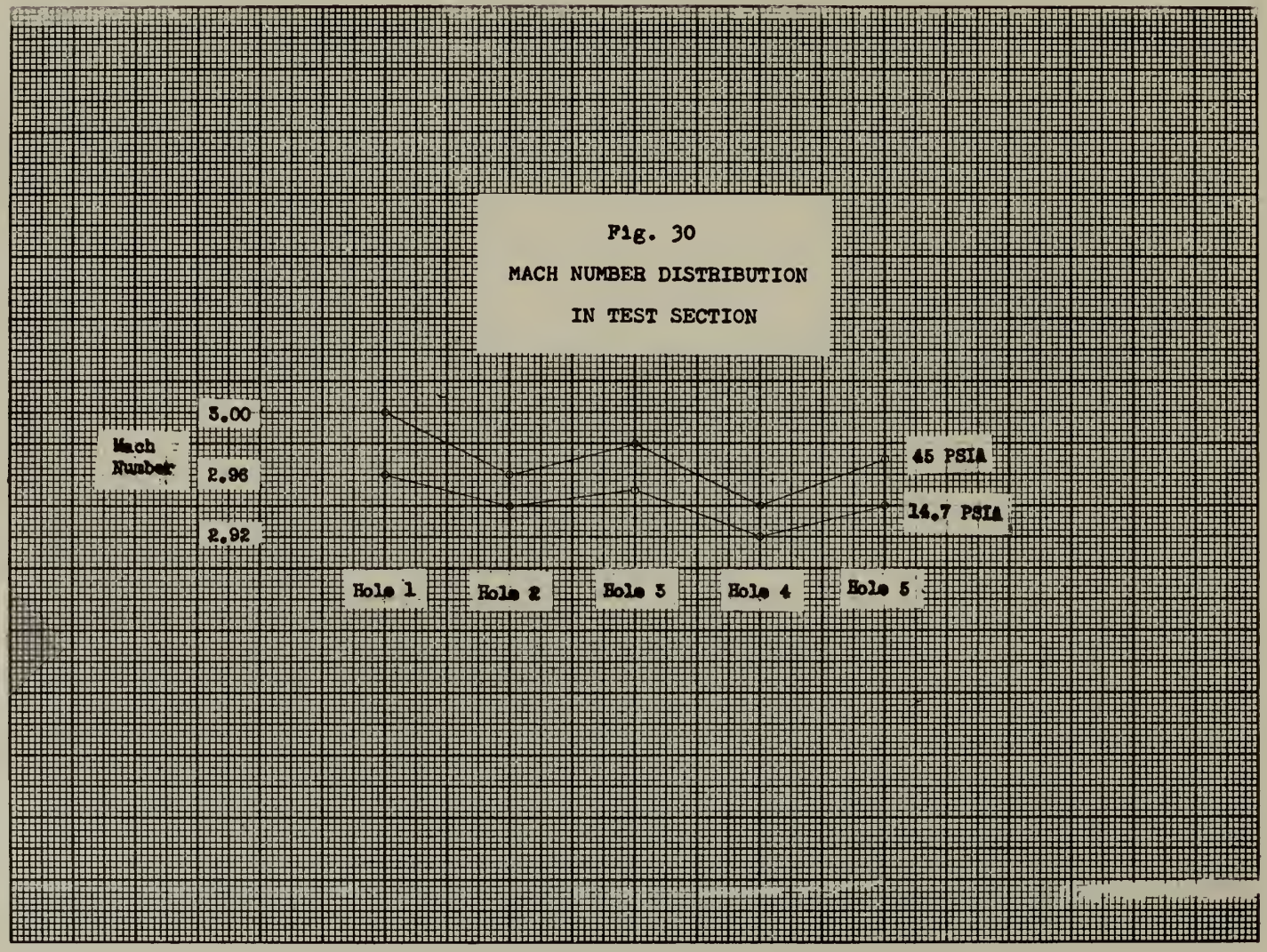

Fig. 30

MACH NUMBER DISTRIBUTION

IN TEST SECTION

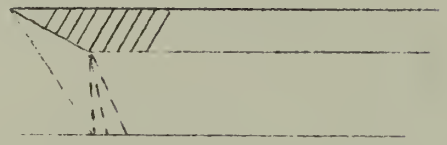

IMPULSE TYPE SHOCK

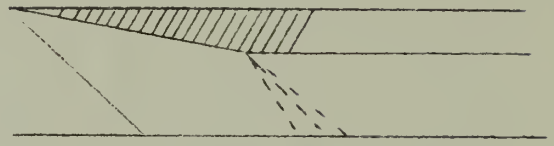

STEP TYPE SHOCK

FIG. 31

TYPES OF SHOCK WAVES

APPENDIX A

Calculations to find position of shock impingement on flat plate.

1. When the wedge was in its most downstream position, its leading edge was found to be 1.033 in. downstream of the leading edge of the flat plate.
2. Distance vertically between the leading edge of a wedge and the flat plate = .878 in.
3. At Mach 3.0, for 10° deviation of flow:

   wave angle = 27.4°

   $\tan 27.4^{\circ} = .518$

   $x = \frac{.878}{.518} = 1.694$ "
4. The shock struck the flat plate 1.694" downstream of the nose of the wedge.
5. Adding (1) and (3) gave 2.727". Hence, the shock struck the flat plate 2.727" downstream of the leading edge of the flat plate.
6. To find the distance, the wedge must move forward to place the shock on the fifth hole downstream, since the fifth hole was 1.725" from the leading edge:

   $$\begin{array}{r} 2.727 \\ 1.725 \\ \hline 1.002" \end{array}$$

   Hence the wedge had to be moved forward 1.002" to strike the fifth hole. The wedge would be moved .25" forward each time to strike succeeding holes upstream.

7. For the 5° wedge, at Mach 3,

$$\text{wave angle} = 23^{\circ}$$

$$\tan 23^{\circ} = .424$$

$$x = \frac{.878}{.424} = 2.070"$$

8. Hence the shock struck the flat plate 3.103" downstream of the leading edge, and to strike the fifth hole the wedge would be moved forward 1.378". For each succeeding hole forward, the wedge would be moved forward .25".

APPENDIX B

Sample calculations to determine the interaction distance upstream by the method of Ref. 3.

Hole 1, 5° wedge, 14.7 psia

$X_o = .725"$ Adding: 1.047

$d = 1.047"$ $\underline{.725}$

$1.772"$

Therefore shock impinged at 1.772" from leading edge, when interaction affected hole 1.

For Mach 3,

$$\delta = 8.9 \frac{X}{R_x^{\frac{1}{2}}}$$ (See section on "Upstream Interaction Distance")

$x = 1.772"$

$R_x = 364{,}000$ (based on total pressure of 14.7 psia and 70° F)

$$\delta_I = \frac{8.9\ (1.772)}{(36.4)(10^4)^{\frac{1}{2}}} = \frac{8.9\ (1.772)}{(6.04)(10^2)} = 2.61\ (10^{-2})"$$

$$\frac{d}{\delta_I} = \frac{1.047}{2.61}\ (10^2) = 40.1$$

Thesis
K727 Koepcke 35893
Interaction between laminar boundary layers and shock waves with separation of flow.